Symplectic Reaction in Olivine and the Controls of Intergrowth Spacing in Symplectites

Article *in* Journal of Petrology · February 2000

DOI: 10.1093/petrology/41.2.285 · Source: OAI

2 authors, including:

Andrew D Chambers
University of Birmingham
11 PUBLICATIONS **259** CITATIONS

SEE PROFILE

JOURNAL OF PETROLOGY | VOLUME 41 | NUMBER 2 | PAGES 285–304 | 2000

Symplectic Reaction in Olivine and the Controls of Intergrowth Spacing in Symplectites

J. R. ASHWORTH* AND A. D. CHAMBERS[6]

SCHOOL OF EARTH SCIENCES, UNIVERSITY OF BIRMINGHAM, EDGBASTON, BIRMINGHAM B15 2TT, UK

RECEIVED JANUARY 6, 1999; REVISED TYPESCRIPT ACCEPTED JULY 23, 1999

Symplectite growth is analysed in terms of non-equilibrium thermodynamics and maximum rate of energy dissipation. For a given reaction, the spacing λ of lamellae or rods is predicted to be proportional to the cube root of $L\delta/v$, *where* v *is reaction rate and* L *is the Onsager diffusion coefficient of a reference element in the reaction front of width* δ. *The result is comparable with, but not identical to, metallurgical theory for discontinuous precipitation in alloys. It is reasoned that concentration-gradient constraints place a lower limit on* λ, *which depends on grain-boundary energy* γ. *An upper limit* $\gamma \sim 0{\cdot}3\ J/m^2$ *is thus estimated using literature data from experimental oxidation of olivine. Combined with new observations on exsolution symplectites in olivine from the Lilloise intrusion, Greenland, this suggests that the exsolution reaction took place above 800°C. Using previous modelling of a corona with a symplectic layer,* $\gamma \sim 1\ J/m^2$ *is estimated for hornblende–spinel symplectite. The energy driving diffusion plus grain-boundary production in the reaction front was a small proportion of the overall affinity of the corona reaction. The theory explains symplectite growth over a wide range of igneous and metamorphic temperatures and timescales.*

KEY WORDS: *discontinuous precipitation; energy dissipation; grain-boundary energy; olivine; symplectite*

INTRODUCTION

It is of general interest in petrology to interpret textures in terms of the energy terms controlling them, with approximate quantification where possible. Although processes such as nucleation are energetically important in some reactions, many other textures are more influenced by diffusion. Here we develop a general theory for a common texture of that type, termed symplectic. Symplectites are mineral intergrowths produced by solid-state reaction (Sederholm, 1916), the grains being elongated perpendicular to the reaction front at which the product minerals grew from a single reactant mineral. The fine-scale, approximately periodic spacing of intergrowth reflects difficult diffusion of some chemical elements. Close analogies have been noted with discontinuous precipitation (also known as cellular precipitation) in alloys (Voll, 1982; Boland & van Roermund, 1983; Mongkoltip & Ashworth, 1983; Boland & Otten, 1985). An example of a rod symplectite, with the minor mineral as rods in the major (host) mineral, is myrmekite (quartz rods in plagioclase). Alternatively, the minor mineral can be lamellar. Many symplectites occur in metamorphic coronas (Sederholm, 1916), which are reaction rims produced between two reactant minerals. The finer the intergrowth, the shorter the diffusion range but also the more grain-boundary area in the symplectite. The scale must be determined by a balance involving diffusive energy dissipation and grain-boundary energy. This paper presents a theory of that balance. Semi-quantitative interpretations follow, for a metamorphic example using literature data, and for symplectic inclusions in igneous olivine using new observations.

In olivine, symplectites of clinopyroxene and magnetite are attributed to exsolution (Moseley, 1984). Another process, oxidation, has produced symplectites of Fe oxide or Fe,Mg oxide with silica or Fe,Mg silicate in many igneous olivines (Haggerty & Baker, 1967; Putnis, 1979; Johnston & Stout, 1984). Reaction with atmospheric

*Corresponding author. Telephone: (44) 121 414 3618. e-mail: J.R.Ashworth@bham.ac.uk

oxygen at high temperatures can be rapid, for example in lavas (Haggerty & Baker, 1967) and in interplanetary dust particles approaching Earth (Rietmeijer, 1996). Such reactions are therefore amenable to experimental study (Champness, 1970; Kohlstedt & Vander Sande, 1975; Brewster & O'Reilly, 1988). Natural symplectites in olivine are attractive for research because their geometry tends to be simple (lamellar), they form in a system with few major components, and the experimental work aids interpretation. In this context, symplectites of exsolution type were examined in samples from the Lilloise intrusion.

SYMPLECTITES IN OLIVINE FROM THE LILLOISE INTRUSION

The Lilloise is a shallow-level Tertiary mafic intrusion in East Greenland (Chambers & Brown, 1995). The symplectites are found in olivine–chrome spinel cumulates, as thin platelets of clinopyroxene and magnetite parallel to (100) of olivine (Fig. 1a). They occur only in olivine less ferroan than Fo_{74}, and are best developed in the most magnesian olivines ($Fo_{85–87}$). They are absent from extensively fractured and serpentinized rocks, are concentrated near the centres of olivine grains despite a lack of significant zoning of these grains, and tend to be associated with subgrain boundaries (Fig. 1b). These observations suggest that the symplectites grew after some deformation, and in those grains or parts of grains where minor components had been unable to diffuse out of the olivine to grain boundaries or cracks.

Thin-sections cut approximately parallel to (100) show that the symplectite comprises transparent and dark minerals (Fig. 1c). Parts of specimens L5 and L410 were examined by transmission electron microscopy (TEM) after ion-beam thinning. The symplectite minerals were identified by TEM energy-dispersive analysis. The clinopyroxene is close to pure diopside and the magnetite, forming lamellae (Fig. 1d), is nearly pure Fe_3O_4.

The average lamellar spacing measured optically in (100) sections (Fig. 1c) is 4·1 μm (SD 0·8 μm, 43 measurements). As the symplectite grew the lamellae branched (Fig. 1c), so as to preserve approximately constant average spacing. TEM images show smaller spacings (~2·8 μm in Fig. 1d), but this is a small sample and probably biased towards closely spaced lamellae, because these are easiest to find in a TEM search. TEM gives the best estimate of the proportion of magnetite (~20% by volume in Fig. 1d); in optical images, the apparent proportion of the dark mineral is exaggerated by any irregularities in lamellar boundaries or obliquity of these to the direction of view (see Moseley, 1984).

TEM observations on the Lilloise symplectites are entirely consistent with those of Moseley (1984) and Otten (1985) on samples from other intrusions. The reaction is topotactic, i.e. both symplectite minerals have crystallographic orientations related to that of olivine (Moseley, 1984, Table 1), such that the oxygen array is minimally changed between reactant and products. All three minerals have approximately close-packed oxygens. In a close-packed layer, there are three directions of close-packed lines of spheres. In cubic close packing, exemplified by magnetite, the close-packed planes are {111} and the lines of close-packing within them, separated by angles of 60°, are <110> lines. In olivine (Deer *et al.*, 1982), the oxygens are approximately hexagonally close-packed; the close-packing plane is (100) and the lines are in the z direction and $\pm 60°$ from it. In pyroxene (Cameron & Papike, 1981), the approximately close-packed plane is (100) and the lines are [010] and <013>. The observed topotaxy is such that close-packed planes and lines in olivine are inherited in both product minerals. All the grain boundaries, including the reaction front, are semicoherent rather than crystallographically random (non-coherent).

PROCESSES OF SYMPLECTITE PRODUCTION IN OLIVINE

Symplectites of the type described above are attributed to exsolution of minor components from olivine (Moseley, 1984). Ca and Fe^{3+} form clinopyroxene and magnetite, respectively. The overall reaction can be summarized as

$$5\,(Fe,Ca,Mg)^{2+}{}_2SiO_4 + 3\,Fe^{3+}{}_{4/3}SiO_4 \rightarrow$$
(in solid solution in olivine)
$$4\,(Ca,Mg,Fe)Si_2O_6 + 2\,Fe^{2+}Fe^{3+}{}_2O_4.$$
(clinopyroxene; magnetite)

It is possible that some oxidation of Fe^{2+} to Fe^{3+} accompanies exsolution, especially as the Fe^{3+} content of olivine should usually be small (Nakamura & Schmalzried, 1983). The retention of the oxygen sublattice (see previous section), and the low diffusion coefficient of oxygen in olivine (Morioka & Nagasawa, 1991), suggest that oxygen is not added; oxidation can be accomplished by diffusion of electrons and cations:

$$4\,Fe^{2+}{}_2SiO_4 \rightarrow 4\,Fe^{2+}SiO_3 + Fe^{2+}Fe^{3+}{}_2O_4 + 2e^- + Fe^{2+}$$

(see Kohlstedt & Vander Sande, 1975). Fe should diffuse to the edge of the olivine grain, as demonstrated by Mackwell (1992) in experimental oxidation of fayalite. With or without oxidation, then, the proportion of pyroxene to magnetite produced is 3:1 in terms of number of oxygen atoms, and approximately the same in volume terms. This is consistent with the TEM images (Fig. 1d).

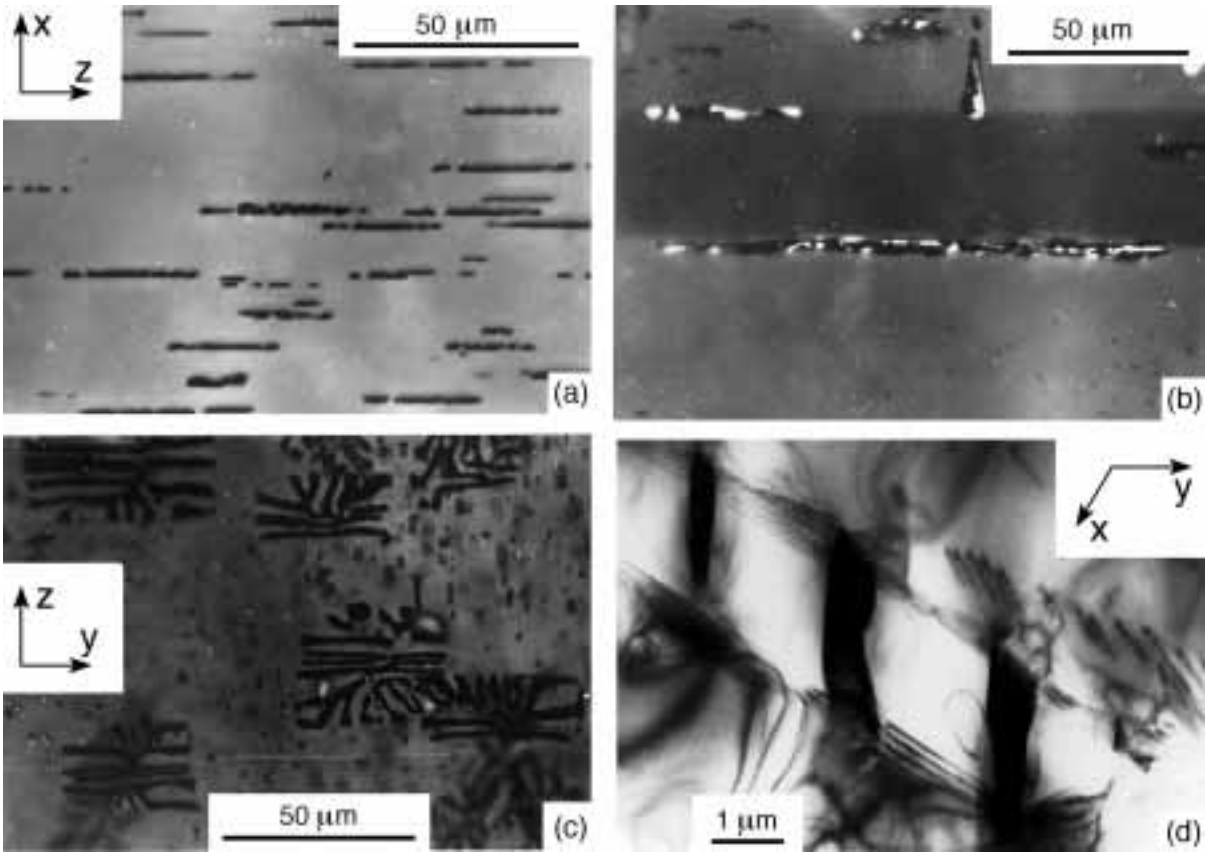

Fig. 1. Symplectites of clinopyroxene and magnetite in Lilloise olivine. (a)–(c) Optical micrographs, (d) TEM image. (a) and (b) show a thin-section cut approximately parallel to (010) so that the symplectite platelets are viewed edgewise. (a) Plane-polarized light. (b) Oblique polars, showing subgrain structure (bands of different grey shade) in olivine, with platelets on subgrain boundaries. (c) A section approximately parallel to the platelet plane, (100) of olivine (plane-polarized light). The clinopyroxene is not distinguishable from the olivine in this view, but the dark magnetite shows the approximately rectangular boundaries of the symplectic platelets. (d) A platelet viewed obliquely by TEM, approximately along the zone axis [312]; projected directions of *x*- and *y*-axes are indicated. Boundaries within the platelet between clinopyroxene and three magnetite lamellae (dark) appear to be non-orthogonal to the (100) platelet boundary, but this is attributable to the obliquity of view.

It is evident from the above that Ca, Fe and Mg can diffuse through the olivine during the reaction, whereas Si is conserved in the reaction front, and the topotaxy implies that oxygen hardly moves at all. The lamellar spacing should be related to the limited movement of silicon and oxygen. Their relative immobility is consistent with the smaller diffusion coefficients of Si and O, relative to divalent cations, in bulk olivine (Morioka & Nagasawa, 1991).

Other symplectites in olivine are attributed simply to oxidation. In a pure oxidation reaction producing silica and iron oxide, the proportions of the two minerals should be approximately equal (they contain equal numbers of oxygen atoms):

$$2\ Fe^{2+}{}_2SiO_4 \rightarrow 2\ SiO_2 + Fe^{2+}Fe^{3+}{}_2O_4 + 2\ e^- + Fe^{2+}$$
magnetite

or

$$3\ Fe^{2+}{}_2SiO_4 \rightarrow 3\ SiO_2 + 2\ Fe^{3+}{}_2O_3 + 4\ e^- + 2\ Fe^{2+}$$
haematite

(see Mackwell, 1992). TEM images (Champness, 1970), are consistent with this. Some examples lack topotaxy (Putnis, 1979). Nevertheless, the oxidation products are so similar to the exsolution type that Si and O are again likely to be slow-diffusing elements.

THEORY OF INTERGROWTH SPACING

This theory uses the principle of maximum rate of energy dissipation (or, equivalently, maximum rate of entropy production), which has been applied to discontinuous precipitation in alloys following the original suggestion of Cahn (1959). It is assumed that reaction rate is

Table 1: Principal symbols

a	$2\gamma V$ (lamellar) or $4\sqrt{(p_R)}\gamma V$ (rod geometry)	J m/mol
b	$KV/L_{Si}\delta$	J s/mol per m^3
c	concentration	mol/m^3
D	Fick's Law diffusion coefficient, $-J/(dc/dx)$	m^2/s
$(-\Delta G)$	affinity of overall reaction	J/mol
$(-\Delta G)_{diff}$	the diffusive part of $(-\Delta G)_{rf}$	J/mol
$(-\Delta G)_{ext}$	the part of $(-\Delta G)$ dissipated outside the reaction front	J/mol
$(-\Delta G)_{gb}$	the part of $(-\Delta G)_{rf}$ deposited in grain boundaries	J/mol
$(-\Delta G)_{rf}$	the part of $(-\Delta G)$ driving processes inside the reaction front	J/mol
J	diffusive flux	mol/m^2 per s
$(k_H)_i$	number of moles of element i added (per m^3 symplectite produced) to the reaction front adjacent to host (major) mineral of symplectite	mol/m^3
$(k_L)_i$	number of moles of element i added (per m^3 symplectite produced) to the reaction front adjacent to minor, lamellar mineral of symplectite	mol/m^3
$(k_R)_i$	number of moles of element i added (per m^3 symplectite produced) to the reaction front adjacent to minor, rod mineral of symplectite	mol/m^3
K	constant in equation (5) for $(-\Delta G)_{diff}$ for a particular symplectite	mol^2/m^6
L	Onsager diffusion coefficient, $-J/(d\mu/dx)$	mol^2/J per m per s
N	number of grain boundaries per metre of line transect	/m
n_{ij}	number of moles of element i per mole of mineral j	
p_L	volume proportion of lamellar mineral in lamellar symplectite	
p_R	volume proportion of rod mineral in rod symplectite	
R	gas constant	J/mol per K
s	constant ratio of $(-\Delta G)_{ext}$ to v	J/mol per m s
t	duration of reaction	s
T	temperature	K
$T\sigma$	rate of energy dissipation per unit volume	J/m^3 per s
v	velocity of reaction front	m/s
V	molar volume of symplectite	m^3/mol
γ	grain-boundary energy	J/m^2
δ	reaction-front width	m
λ	spacing of lamellae or rods in symplectite	m
$d\mu/dx$	chemical-potential gradient	J/mol per m
ν_j	stoichiometric coefficient of mineral j	

controlled by diffusion together with the grain-boundary energy term, and is steady state (i.e. short-term fluctuations are discounted, as is generally acceptable for slow petrological reactions; e.g. Ashworth & Sheplev, 1997). Symbols are listed in Table 1. The total affinity $(-\Delta G)$ is constant for a reaction at constant pressure, temperature and mineral compositions. It is divided into the energy that drives processes in the reaction front and the part driving external processes:

$$(-\Delta G) = (-\Delta G)_{rf} + (-\Delta G)_{ext}.$$

In an open system, the important external process is diffusion outside the reaction front, supplying components for symplectite growth. As the chemical-potential gradients driving external diffusion should be proportional to $(-\Delta G)_{ext}$, reaction rate measured by reaction-front velocity v (Fig. 2) should also be proportional to $(-\Delta G)_{ext}$, so that s is a constant in

$$(-\Delta G)_{ext} = sv.$$

Within the reaction front, an example of important

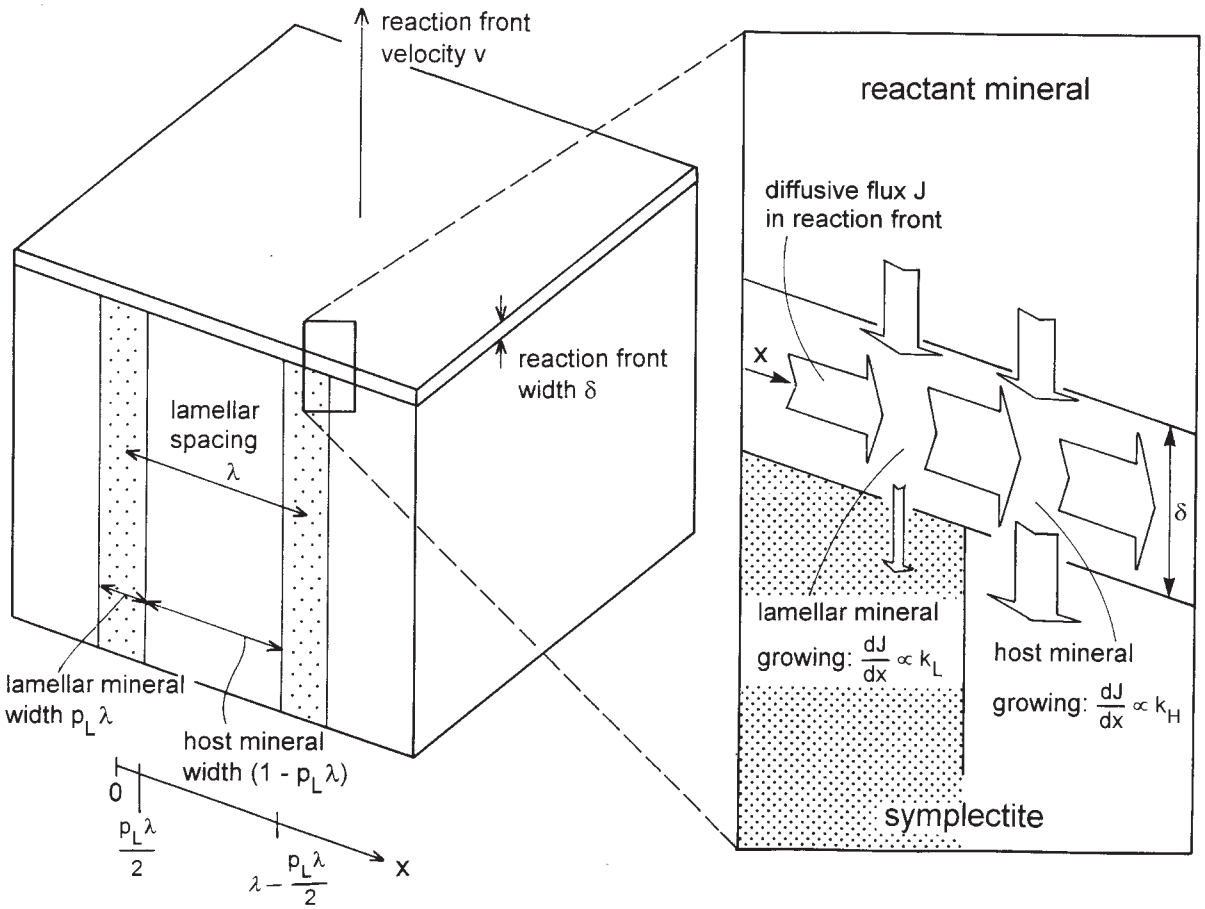

Fig. 2. Idealized geometry of a growing lamellar symplectite. Reaction-front width, δ, is very small [~1–3 nm if comparable with normal grain boundaries (Farver *et al.*, 1994)]. The enlarged diagram at the right schematically shows diffusive flux $\mathcal{J}$, with additions to it as the reactant mineral is consumed and subtractions as the symplectite minerals grow. The flux illustrated, directed from lamella to host region, is that of an element for which the supply from the reactant mineral exceeds deposition in the lamellar product (k_L>0), so that flux increases with distance x opposite the lamellar mineral. Conversely, k_H <0 so that the flux decreases with x opposite the host mineral.

diffusion is that of Si (in the exsolution of magnetite + clinopyroxene from olivine) from the area where magnetite is growing, to be deposited in the pyroxene. The free energy associated with energy dissipation by reaction-front diffusion, $(-\Delta G)_{\text{diff}}$, increases with increasing spacing of the products, whereas the grain-boundary area between the symplectite minerals decreases and thus the energy term $(-\Delta G)_{\text{gb}}$ decreases in the balance of energy at the reaction front

$$(-\Delta G)_{\text{rf}} = (-\Delta G)_{\text{diff}} + (-\Delta G)_{\text{gb}}.$$

These energies will now be examined for lamellar geometry (rod geometry is treated in the Appendix).

In terms of grain-boundary energy γ and lamellar spacing λ,

$$(-\Delta G)_{\text{gb}} = \frac{2\,\gamma\,V}{\lambda}$$

where molar volume V should be an averaged quantity. With reference to Fig. 2, the diffusive flux $\mathcal{J}$ of an element in the reaction front varies with distance x in the region where the lamellar mineral is growing, thus

$$\frac{\mathrm{d}\mathcal{J}}{\mathrm{d}x} = \frac{v\,k_{\text{L}}}{\delta} \qquad (-p_{\text{L}}\,\lambda/2 \le x \le p_{\text{L}}\,\lambda/2).$$

Here k_{L} (mol/m^3) is the effective difference in concentration of the element between the reactant mineral and the lamellar product. If there is diffusion through either of these, to or from the reaction front, this should be taken into account, but otherwise k_{L} simply reflects the difference in mineral compositions. If k_{H} is the analogous difference between reactant mineral and the host mineral in the symplectite, then in that region of the reaction front

$$\frac{\mathrm{d}\mathcal{J}}{\mathrm{d}x} = \frac{v\,k_{\text{H}}}{\delta} \qquad (p_{\text{L}}\,\lambda/2 \le x \le \lambda - p_{\text{L}}\,\lambda/2).$$

If the system is closed to the element (i.e. there is no external flux),

$$k_H = \frac{-p_L}{1-p_L} k_L \quad (1)$$

and, with no diffusion along the host–lamella grain boundary, there is no discontinuity in $\mathcal{J}$ where the reaction front crosses that boundary (Fig. 3a). The flux changes direction at $x = 0$ and $x = \lambda/2$ (Fig. 3a). Between these points,

$$\mathcal{J} = \frac{v\, k_L\, x}{\delta} \qquad (0 \le x \le p_L\, \lambda/2)$$

$$\mathcal{J} = \frac{-v\, k_H\, (\lambda/2 - x)}{\delta} \qquad (p_L\, \lambda/2 \le x \le \lambda/2).$$

If diffusion obeys Fick's Law, flux is related to concentration gradient by the diffusion coefficient D:

$$\mathcal{J} = -D\frac{dc}{dx}.$$

Concentration varies thus, from $c = c_0$ at $x = 0$:

$$c = c_0 - \frac{v\, k_L\, x^2}{2\, D\, \delta} \qquad (0 \le x \le p_L\, \lambda/2)$$

$$c = c_0 - \frac{v\, k_L\, p_L{}^2\, \lambda^2}{8\, D\, \delta} - \frac{v\, k_H}{2\, D\, \delta}\left[\left(\frac{\lambda}{2} - x\right)^2 - (1 - p_L)^2 \frac{\lambda^2}{4}\right] \qquad (p_L\, \lambda/2 \le x \le \lambda/2).$$

This simplifies in a closed system, using equation (1):

$$c = c_0 - \frac{v\, k_L\, p_L}{2\, D\, \delta}\left\{\frac{\lambda^2}{4} - \frac{[(\lambda/2) - x]^2}{1 - p_L}\right\} \qquad (p_L\, \lambda/2 \le x \le \lambda/2).$$

For an element diffusing from lamella to host, c_0 is the maximum concentration, and the minimum, at $x = \lambda/2$ (Fig. 3b), is

$$c_{min} = c_0 - \frac{v\, k_L\, p_L\, \lambda^2}{8\, D\, \delta}. \quad (2)$$

Obviously, c_{min} cannot be less than zero. This gives a concentration limit

$$\frac{D\, \delta}{v} > \frac{k_L\, p_L\, \lambda^2}{8\, c_0}. \quad (3)$$

Indeed, c_{min} for a major element is unlikely to approach zero. For example, during symplectite growth in olivine, c_{min} for Si occurs in the boundary between olivine and silica or pyroxene, and should remain at a level comparable with the Si content of these minerals. Therefore, the concentration limit should not be closely approached.

The following treatment of diffusive energy dissipation uses the Onsager diffusion coefficient L, which relates flux $\mathcal{J}$ to chemical-potential gradient:

$$\mathcal{J} = -L\frac{d\mu}{dx}.$$

A useful approximation, given that c should not approach zero, is

$$L = \frac{c\, D}{RT}.$$

If L is measured at $c = c_0$, equation (2) can be written

$$\frac{c_0 - c_{min}}{c_0} = \frac{v\, k_L\, p_L\, \lambda^2}{8\, RT\, L\, \delta}.$$

The condition for the concentration limit (3) not to be approached becomes

$$\frac{L\, \delta}{v} > \frac{k_L\, p_L\, \lambda^2}{8\, RT}. \quad (4)$$

Using the principles of irreversible thermodynamics (Fisher & Lasaga, 1981), the rate of energy dissipation per unit volume is $\mathcal{T}\sigma = -\mathcal{J}(d\mu/dx)$:

$$\mathcal{T}\sigma = \frac{v^2\, k_L{}^2\, x^2}{L\, \delta^2} \qquad (0 \le x \le p_L\, \lambda/2)$$

$$\mathcal{T}\sigma = \frac{v^2\, k_H{}^2\, (\lambda/2 - x)^2}{L\, \delta^2} \qquad (p_L\, \lambda/2 \le x \le \lambda/2).$$

Multiplying by $\delta.dx$ and integrating from $x = 0$ to $x = \lambda/2$ gives the energy dissipation rate in an area of reaction front measuring $\lambda/2$ by 1 m. Then dividing by $v\lambda/2$ gives the energy dissipated per cubic metre of symplectite produced, and multiplying by V gives $(-\Delta G)_{diff}$ per mole of symplectite:

$$(-\Delta G)_{diff} = \frac{2\, v\, V}{\lambda\, L\, \delta}\left[k_L{}^2 \int_0^{p_L\lambda/2} x^2 dx + k_H{}^2 \int_{p_L\lambda/2}^{\lambda/2} (\lambda/2 - x)^2 dx\right]$$

$$= \frac{v\, V\, \lambda^2}{12\, L\, \delta}\left[p_L{}^3\, k_L{}^2 + (1 - p_L)^3\, k_H{}^2\right].$$

The above applies to a single diffusing element. For the general case of several diffusing elements i,

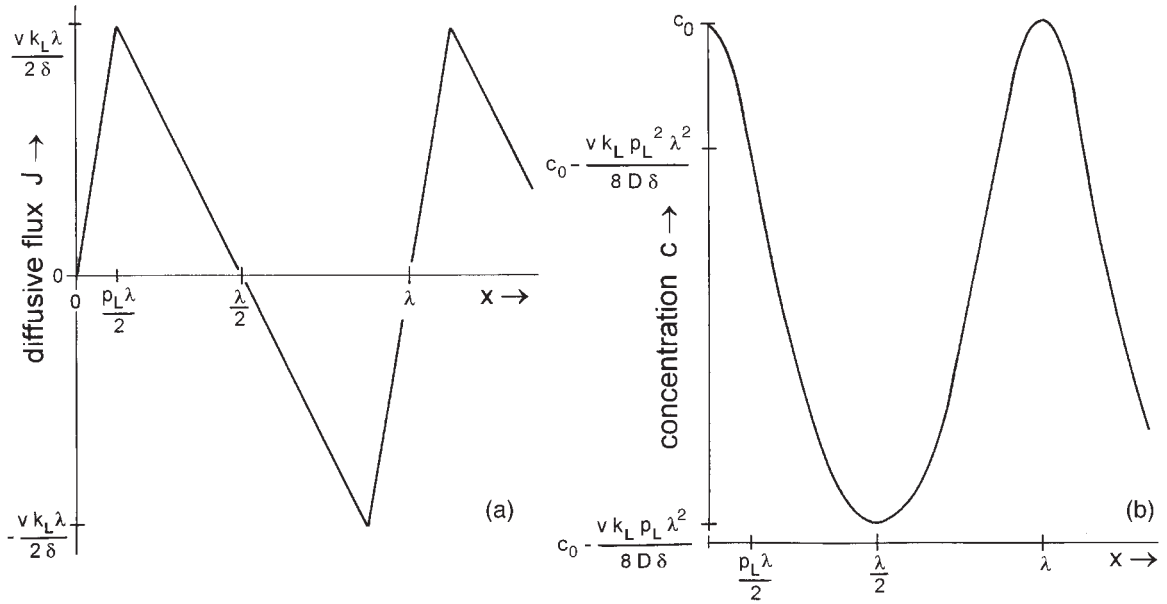

Fig. 3. Variation of flux (a) and concentration (b) with distance x in the reaction front of Fig. 2, for an element that diffuses from the lamella region (to be deposited in the host mineral). It is assumed that this element diffuses in the reaction front only, i.e. equation (1) applies.

$$(-\Delta G)_{\text{diff}} = \frac{K v V \lambda^2}{L_{\text{Si}} \delta} \tag{5}$$

where

$$K = \frac{1}{12}\left[p_{\text{L}}{}^3 \sum_i (k_{\text{L}})_i^2 \frac{L_{\text{Si}}}{L_i} + (1-p_{\text{L}})^3 \sum_i (k_{\text{H}})_i^2 \frac{L_{\text{Si}}}{L_i} \right]. \tag{6}$$

(The use of ratios L_{Si}/L_i is convenient for the interpretation of coronas below.) K effectively measures the strength of diffusive segregation between the product minerals.

Maximum rate of energy dissipation

Summarizing the working above and in the Appendix,

$$(-\Delta G)_{\text{ext}} = sv, \qquad (-\Delta G)_{\text{gb}} = \frac{a}{\lambda},$$

$$(-\Delta G)_{\text{diff}} = bv\lambda^2 \tag{7}$$

$$(-\Delta G) = sv + \frac{a}{\lambda} + bv\lambda^2 \tag{8}$$

where

$$a = 2\gamma\, V(\text{lamellar}) \text{ or } 4\sqrt{(p_{\text{R}})}\gamma\, V(\text{rod})$$

and

$$b = \frac{KV}{L_{\text{Si}}\delta}.$$

For a given reaction under fixed conditions [i.e. for given values of a, b, s and $(-\Delta G)$], values of v and λ can be found that maximize either reaction rate or rate of energy dissipation. This is illustrated in Figs 4 and 5, by treating v and λ as variables, although in physical reality they cannot vary arbitrarily (it will be argued that they should, in fact, be constrained to the values for maximum energy dissipation rate, demonstrated by Figs 4c and 5b). In Fig. 4, with reaction rate v treated as variable, the solution shown for λ (Fig. 4a) is the largest root of the cubic equation (8), which gives the largest $(-\Delta G)_{\text{diff}}$ and hence the fastest energy dissipation at given v. Figure 5 shows this solution for λ (as the large filled circle) at two selected values of v. In Fig. 4a, as v increases, the faster transport of material requires shorter diffusion distances, so λ decreases. This implies more grain boundaries, so $(-\Delta G)_{\text{gb}}$ increases (Fig. 4b); $(-\Delta G)_{\text{ext}}$ increases proportionally to v, whereas $(-\Delta G)_{\text{diff}}$ decreases, maintaining constant sum $(-\Delta G)$. Figure 4 shows a velocity limit, beyond which there is no solution for λ; the sum of $(-\Delta G)_{\text{diff}}$ and $(-\Delta G)_{\text{gb}}$ would exceed the available energy $(-\Delta G) - sv$ for all λ. At this velocity limit, v_{max} (Fig. 5a), the above sum just falls to the required amount at one value of λ, where

$$2\,(-\Delta G)_{\text{diff}} = (-\Delta G)_{\text{gb}}. \tag{9}$$

This situation maximizes reaction rate, but does not quite maximize the rate of energy dissipation. The latter

involves the diffusive term $(-\Delta G)_{ext}$ as well as $(-\Delta G)_{diff}$. We require the maximum of

$$v[(-\Delta G)_{ext} + (-\Delta G)_{diff}] = v^2(s + b\lambda^2).$$

Differentiating with respect to v and equating to zero,

$$s + b\lambda\left(\lambda + v\frac{d\lambda}{dv}\right) = 0.$$

Also, differentiating equation (8) with $(-\Delta G)$ constant,

$$\frac{d\lambda}{dv} = \frac{-(b\lambda^2 + s)}{2bv\lambda - (a/\lambda^2)}.$$

Combining these two equations with equations (7),

$$(-\Delta G)_{ext} + (-\Delta G)_{diff} = (-\Delta G)_{diff}\left[\frac{(-\Delta G)_{diff} + (-\Delta G)_{ext}}{2(-\Delta G)_{diff} - (-\Delta G)_{gb}}\right]$$

and rearrangement gives

$$(-\Delta G)_{diff} = (-\Delta G)_{gb}. \quad (10)$$

Half of the reaction-front energy $(-\Delta G)_{rf}$ goes into each term. This situation is illustrated graphically in Figs 4c and 5b. The result remains valid in a completely closed system, i.e. if $(-\Delta G)_{ext}$ is zero. Equating $(-\Delta G)_{diff}$ with $(-\Delta G)_{gb}$ in equations (7) gives the solution for λ:

$$\lambda^3 = \frac{a}{bv} = \frac{2\gamma L_{Si}\delta}{Kv} \text{ (lamellar geometry)}$$

or

$$\frac{4\sqrt{(p_R)}\gamma L_{Si}\delta}{Kv} \text{ (rod geometry)} \quad (11)$$

at maximum rate of energy dissipation. Equation (11) is the key result for the Applications sections below.

Although inequality (4) indicates that the concentration limit would be approached with increasing λ if other quantities could be held constant, relation (11) among these quantities shows that the concentration limit actually sets a minimum value of λ for a given reaction. Combining equation (11) with inequality (4) for the lamellar closed-system case shows that, for the concentration limit not to be approached for element i,

$$\lambda > \frac{L_{Si}}{L_i}\frac{(k_L)_i p_L \gamma}{4KRT}. \quad (12)$$

The rod-geometry equivalent, not necessarily in a closed system, from inequality (A1) of the Appendix, is

$$\lambda > \frac{L_{Si}}{L_i}\frac{\sqrt{(p_R)}\gamma}{4KRT}[(k_R)_i p_R - (k_H)_i(p_R - \ln p_R - 1)]. \quad (13)$$

COMPARISON WITH DISCONTINUOUS PRECIPITATION IN ALLOYS

In discontinuous precipitation, an alloy decomposes to two purer metals in a rod or lamellar intergrowth, when held at a temperature below the relevant solvus. Zoning is detectable in the host product, and reflects the concentration profile in the reaction front. In the petrological analogue, such zoning is not generally possible. Let us consider the growth of myrmekite. In the reaction front, Na and Ca must both diffuse away from growing quartz. Their chemical-potential gradients are therefore in the same direction, whereas the only possible zoning in the growing plagioclase would have Na and Ca varying antithetically. In some symplectites, zoning parallel to the reaction front is observed, but can possibly be attributed to modification of the minerals after their growth (Ashworth *et al.*, 1992).

Discontinuous precipitation in metals generally does not require diffusion beyond the reaction front, so $(-\Delta G)_{rf}$ equals the total free energy change $(-\Delta G)$. This may also be true for some symplectite-forming reactions, such as the decomposition of augite into two pyroxenes studied by Boland & Otten (1985). However, in the metals, the zoning means that $(-\Delta G)$ is only a fraction of the free energy change $(-\Delta G)_{eq}$ that would be realized if equilibrium, unzoned products grew: this fraction is denoted $P(-\Delta G)_{eq}$. The overall energy balance is

$$P(-\Delta G)_{eq} - (-\Delta G)_{gb} = (-\Delta G)_{diff} \quad (14)$$

and P is a function of v and λ (Cahn, 1959), decreasing as λ and v increase.

The reactions in metals can be studied experimentally. Commonly, estimates are available for $(-\Delta G)_{eq}$ and γ. Zoning is measured by analytical TEM (Zieba & Gust, 1998). From the zoning profiles, P can be calculated. This depends on the thermodynamic model used for solid solution; nevertheless, $P(-\Delta G)_{eq}$ and $(-\Delta G)_{gb}$ can be estimated more readily than $(-\Delta G)_{diff}$, and the latter is not usually calculated explicitly. The conditions for maximum $v(-\Delta G)_{diff}$ are found by maximizing v times the left-hand side of equation (14). Solorzano & Purdy (1984) demonstrated a clearly defined maximum as a function of v at constant λ. Bögel & Gust (1988) reasoned that v and λ can be optimized simultaneously. They obtained the result that $(-\Delta G)_{gb}$ is twice $(-\Delta G)_{diff}$ at maximum energy dissipation rate, independently of the model used for P. This is comparable with, but clearly not identical to the present result: it corresponds to equation (9) for maximum reaction rate in this work, rather than equation (10) for maximum rate of energy dissipation. The different result of Bögel & Gust (1988) is not due to zero $(-\Delta G)_{ext}$, which did not invalidate equation (10): the difference lies in the zoning.

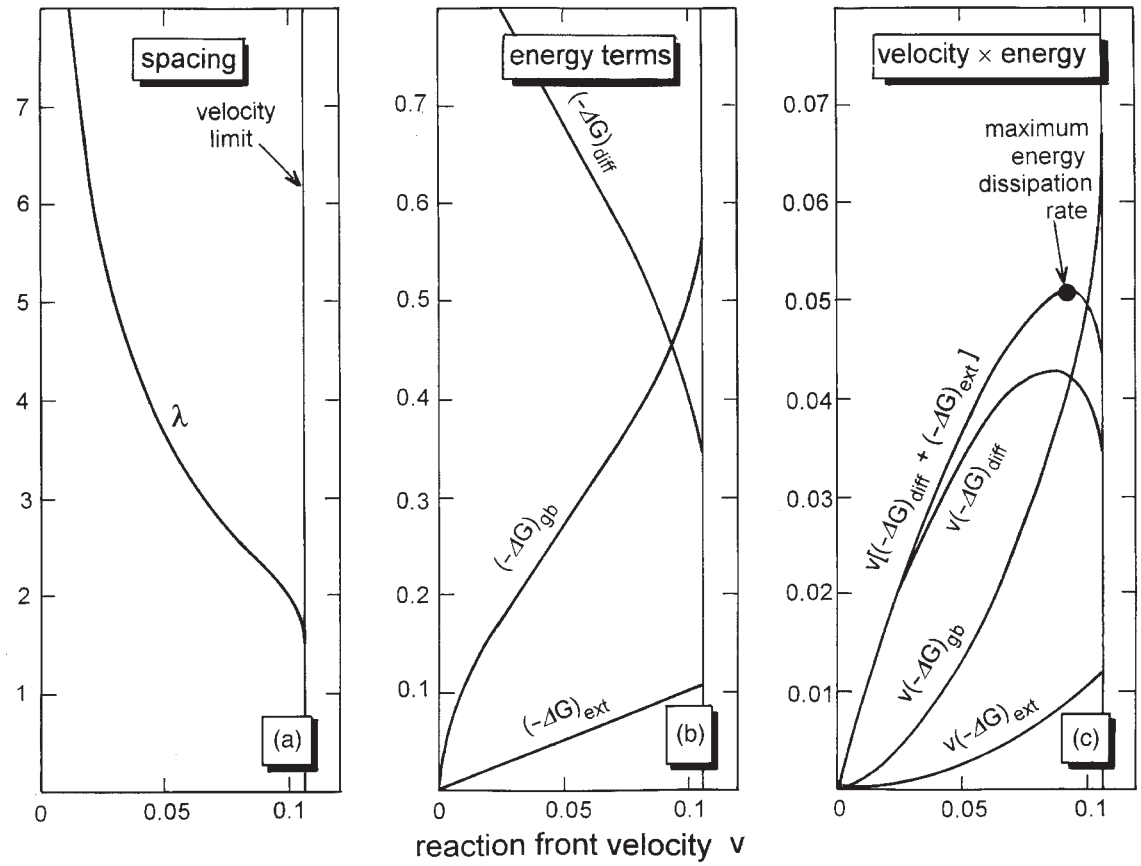

Fig. 4. Hypothetical variation in quantities calculated by allowing reaction rate v to vary, for a symplectite with fixed values of a, b, s and $(-\Delta G)$ (all arbitrarily set to unity). (a) Optimum value of spacing λ, given by the largest root of equation (8). (b) Energy quantities $(-\Delta G)_{gb}$, $(-\Delta G)_{diff}$ and $(-\Delta G)_{ext}$ corresponding to the λ variation shown in (a), calculated from equations (7). (c) v × energy, showing the maximum in energy dissipation rate $v[(-\Delta G)_{diff} + (-\Delta G)_{ext}]$.

Bögel & Gust (1988) claimed good agreement between their theory and experiments, particularly at small departures from equilibrium. However, data of Duly *et al.* (1994) seem to require revision of the theory of Bögel & Gust (1988). The metallurgical problem may be complicated by additional factors, such as non-steady-state variations in v between zero and about five times average velocity (Abdou *et al.*, 1996). These may be related to variations in the zoning pattern, in an oscillatory manner perpendicular to the reaction front (Zieba & Gust, 1998, p. 80).

APPLICATION TO SYMPLECTITES IN OLIVINE

For a natural symplectite, the growth rate v could be estimated from equation (11) and measurements of λ, if γ, $L_{Si}\delta$ and K were known. Although there is an additional grain-boundary energy associated with the large boundary area between platelets and olivine [their shape being presumably controlled by low-energy semicoherent (100) boundaries], this does not depend on λ and need not be considered here.

A value for K can be calculated by equation (6) if the relative magnitudes of diffusion coefficients for the major diffusing elements can be estimated. The lowest diffusion coefficients should be for Si and O; as O is inferred not to diffuse at all, the diffusion term is considered to be dominated by Si. Using the quantities for Si alone, equation (6) becomes

$$K = \frac{1}{12}\left[p_L{}^3\,(k_L)_{Si}{}^2 + (1-p_L)^3\,(k_H)_{Si}{}^2\right].$$

It is reasonable to assume a closed system for Si, so equation (1) applies, giving

$$K = \frac{p_L{}^2\,(k_L)_{Si}{}^2}{12}. \qquad (15)$$

From stoichiometry, $p_L \approx 0{\cdot}25$ (see section on processes

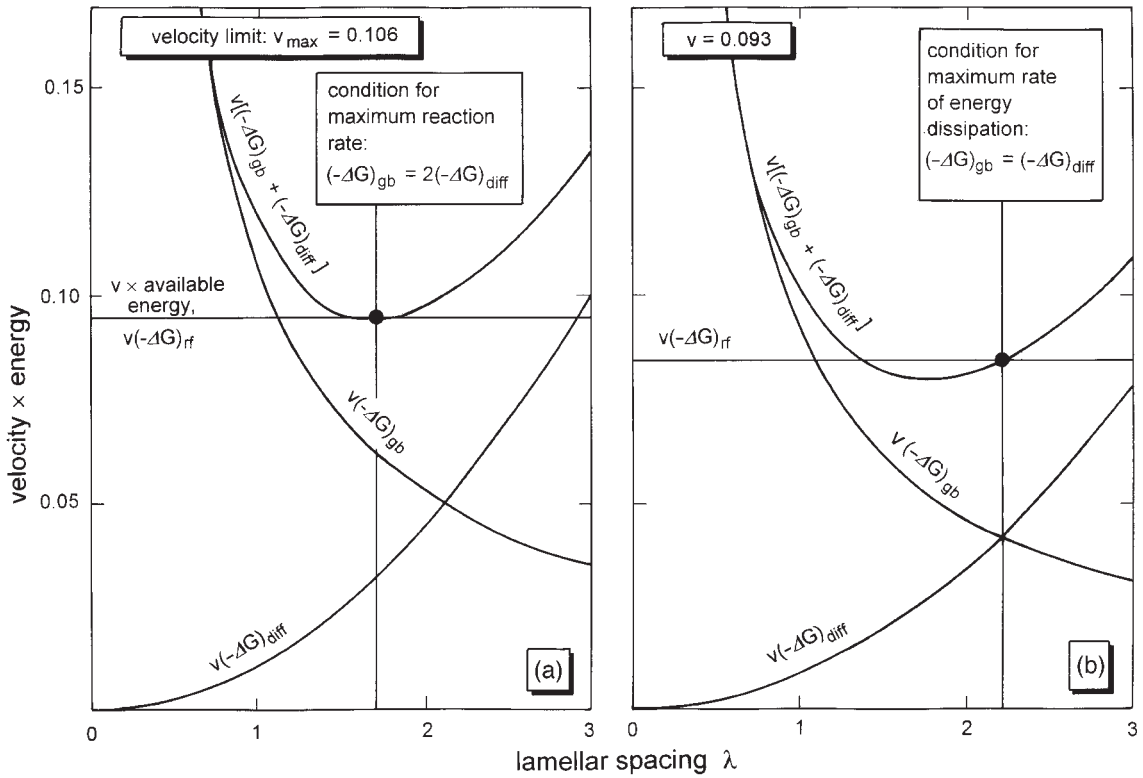

Fig. 5. Quantities calculated from equations (7) by hypothetically varying λ at two fixed values of v. The fixed values of a, b, s and $(-\Delta G)$ are the same as in Fig. 4. The energy quantities are multiplied by v to show the rate of energy dissipation in the reaction front, $v(-\Delta G)_{\text{diff}}$. The energy available at the reaction front, $(-\Delta G)_{\text{rf}}$, is constant at given v, equal to $(-\Delta G) - sv$. Physically possible values of λ are those for which this value of $(-\Delta G)_{\text{rf}}$ equals the sum of the calculated $(-\Delta G)_{\text{gb}}$ and $(-\Delta G)_{\text{diff}}$. (a) At the velocity limit $v_{\max}$, the only possible value of λ is such that $(-\Delta G)_{\text{gb}} = 2(-\Delta G)_{\text{diff}}$. (b) At the velocity for maximum rate of energy dissipation, that maximum corresponds to $(-\Delta G)_{\text{gb}} = (-\Delta G)_{\text{diff}}$. Despite the smaller v, the dissipation rate $v(-\Delta G)_{\text{diff}}$ is larger at this point than at the permitted value of λ in (a).

above). As no Si enters magnetite, $(k_{\text{L}})_{\text{Si}}$ equals the concentration of Si in olivine (neglecting volume change in reaction). The molar volume of olivine is approximately $4{\cdot}4 \times 10^{-5}$ m^3/mol (Holland & Powell, 1998) and contains one mole of Si, so $(k_{\text{L}})_{\text{Si}} \approx 2{\cdot}3 \times 10^4$ mol/m^3, and $K \approx 2{\cdot}8 \times 10^6$ mol^2/m^6.

The concentration limit (3) places some constraints on the interpretation of the Lilloise symplectites. It is assumed that the maximum concentration, c_0, approximates that of Si in olivine, which also equals $(k_{\text{L}})_{\text{Si}}$ so that $c_{\min} > 0$ implies

$$\frac{8\, D_{\text{Si}}\delta}{v\, p_{\text{L}}\lambda^2} > 1. \qquad (16)$$

It can immediately be shown that D_{Si} in the reaction front must exceed that in bulk olivine. The largest values reported for the latter (Houlier *et al.*, 1990) are around 8×10^{-22} m^2/s at 1250°C (as high an initial temperature as could be considered for the Lilloise intrusion). Grain-boundary widths δ are ~1–3 nm for non-coherent boundaries in olivine (Farver *et al.*, 1994), and should be smaller for semicoherent ones. These values would lead to a maximum of $2{\cdot}4 \times 10^{-30}$ m^3/s for $D_{\text{Si}}\delta$ which, with $p_{\text{L}} \approx 0{\cdot}25$ and $\lambda \approx 4{\cdot}1$ μm, would mean $v < 5 \times 10^{-18}$ m/s from inequality (16). The platelets would take more than 10^5 years to grow 20 μm. This is longer than would be available at temperatures near 1250°C (maximum possible intrusion temperature).

To proceed further requires some constraint on γ or $L_{\text{Si}}\delta/v$. Literature values for grain-boundary energies in minerals are scarce, but Spry (1969) tabulated surface energies that are likely to be about three times the values of interface (grain-boundary) energies, and indicate γ in the range 0·03–2 J/m^2. Hay & Evans (1988) experimentally estimated $\gamma = 130$ mJ/m^2 in calcite at 800°C. By treating grain boundaries as dislocation arrays, Penn *et al.* (1999) calculated $\gamma = 0{\cdot}3$–$1{\cdot}0$ J/m^2 in sillimanite (varying with misorientation angle between the grains). Combining this type of theory with experimental data on solid–liquid dihedral angles, Cooper & Kohlstedt (1982) estimated $\gamma = 0{\cdot}9 \pm 0{\cdot}4$ J/m^2 for high-angle (misorientation >15°) grain boundaries in olivine. Also in olivine, they found $\gamma = 0{\cdot}08 \pm 0{\cdot}02$ J/m^2 for low-angle (0·2°) subgrain boundaries, in which the individual

dislocations are easily resolved in TEM. The semicoherent boundaries considered here, in which individual dislocations can also be resolved (Moseley, 1984, Fig. 2e), are probably intermediate in kind between low-angle subgrain boundaries and incoherent grain boundaries. This is consistent with metallurgical analogy, which indicates that a semicoherent boundary might have about one-fifth the energy of a non-coherent one (Kretz, 1994, p. 302), i.e. possibly in the range 0·006–0·4 J/m^2.

Some further information can be gleaned from the oxidation experiments in olivine. These have mostly produced symplectites comprising iron oxide and silica (references in Table 2). They provide a constraint on γ as follows. Although some diffusion of oxygen seems possible in these reactions, it is assumed that Si diffusion still dominates the energetics. For a symplectite of iron oxide + silica, $p_L \approx 0{\cdot}5$ by stoichiometry (see section on processes above), $(k_L)_{Si} \approx 2{\cdot}3 \times 10^4$ mol/m^3 as in the exsolution case, and $K \approx 1{\cdot}1 \times 10^7$ mol^2/m^6 from equation (15). From some photomicrographs, λ can be estimated (Table 2). Rearrangement of inequality (12) then gives an upper limit for γ, if the concentration limit for Si is not to be approached:

$$\gamma < \frac{4\,K R T \lambda}{k_L\, p_L}. \qquad (17)$$

The low-temperature experiments give the most stringent limits (Table 2). Those of Khisina *et al.* (1995, 1998) are complicated by the production of two oxide minerals, and also 'ferriolivine' between the oxide–silica regions, and so may not represent the simple reaction analysed here. 'Ferriolivine' (the Fe end-member of which is laihunite, $Fe^{2+}{}_{2-3x}Fe^{3+}{}_{2x}SiO_4$) tends to be produced in preference to symplectites in low-temperature oxidation of olivine (<600°C approximately, in air: Kondoh *et al.*, 1985; Khisina *et al.*, 1998). Iishi *et al.* (1997) produced probable symplectites at unusually low temperature (300°C), but in demounted thin-sections immersed in an aqueous medium, where species from that medium enter the grain boundaries and may enhance diffusion so that the concentration limit (16) is satisfied. Reaction to 'ferriolivine' instead of symplectite may reflect approach to the concentration limit, or possibly that λ becomes so small (<10 nm) that symplectites are 'mostly grain boundary' and have higher than normal free energy. The experiment of Champness (1970) at 650°C, which produced the two-phase symplectite without 'ferriolivine', is taken as setting the upper limit to be used here: $\gamma \leq 0{\cdot}3$ J/m^2. This is used in contouring the plot of log λ vs log v (Fig. 6). Admittedly, the energy may be smaller for semicoherent boundaries than for those between haematite and amorphous silica produced by Champness (1970).

Where the size of the symplectite is reported, this and the duration of the experiment give an estimate for v (Table 2). [This obviously varies greatly with experimental conditions: for example, Mackwell (1992) achieved high rates in producing a surface layer of iron oxide + silica, rather than inclusions inside olivine.] Then equation (11) gives an estimate for $\gamma L_{Si}\delta$, which combined with the upper limit for γ gives a lower limit for $L_{Si}\delta$ (Table 2). This indicates that $L_{Si}\delta$ increases strongly with temperature, as would be expected from the Arrhenius law. Because of differences of experimental approach, detailed comparisons are not possible. However, the rough estimates of $L_{Si}\delta$ in Fig. 6 are comparable with separate experimental results on grain-boundary diffusion in olivine. Fisler & Mackwell (1994) and Yund (1997) studied diffusion-controlled growth of an olivine layer. The rate-controlling element is not directly identified, but Si is probably indicated. These studies indicate $D_{Si}\delta \sim 10^{-23}$ m^3/s in non-coherent, dry olivine boundaries at 1000°C, corresponding to $L_{Si}\delta \sim 2 \times 10^{-23}$ mol^2/J per s. At 1400°C in enstatite grain boundaries, results of Fisler *et al.* (1997) give $D_{Si}\delta \sim 10^{-22}$ m^3/s.

For the Lilloise reaction, values $\lambda \approx 4$ μm, $K \approx 2{\cdot}8 \times 10^6$ mol^2/m^6 and $\gamma \leq 0{\cdot}3$ J/m^2 imply $L_{Si}\delta > 3 \times 10^{-10}\, v$. A minimum for v is set by noting that ~1 ky is the maximum time that would be available for reaction in the cooling, shallow-level intrusion. Growth of 20 μm (to give platelet dimensions ~40 μm as in Fig. 1c) then implies $v > 6 \times 10^{-16}$ m^3/s, approximately. This indicates minimum $L_{Si}\delta \sim 10^{-25}$ mol^2/J per s, only two orders of magnitude below the experimentally based estimates at 1000°C. Although the temperature dependence of $L_{Si}\delta$ is not yet well constrained experimentally, indications are that $L_{Si}\delta$ would be $<10^{-25}$ mol^2/J per s at $T < 800$°C (Table 2 and following sections). Thus, the exsolution reaction in the Lilloise olivine probably took place at $T > 800$°C.

APPLICATION TO METAMORPHIC CORONAS

Studies of the distribution of minerals among layers in coronas have led to an understanding of their diffusion-controlled growth (Ashworth & Sheplev, 1997). In one case with a symplectic layer, the ratio $L_{Si}\delta/v$ is fairly well constrained for diffusion through the grain boundaries across layers. Assuming that $L_{Si}\delta$ in the reaction front is approximately the same as in those boundaries, an order-of-magnitude estimate can be obtained for γ. This case is the hornblende–spinel symplectite originally described by Mongkoltip & Ashworth (1983). It grew from plagioclase in a reaction with olivine (Fig. 7). The rocks are troctolites from ~500 Ma gabbroic intrusions in NE Scotland. Unlike the Lilloise, these were emplaced during regional metamorphism, and cooled slowly, undergoing retrograde reaction in the amphibolite facies (Mongkoltip

Table 2: Information from oxidation experiments producing iron oxide + silica from olivine

T (°C)	Reference	Symplectic products	λ (μm)	*v* (m/s)	Approximate upper limit on γ (J/m^2) from inequality (17)	Estimated $\gamma L_{Si}\delta$ (mol^2/ m^2 per s) from equation (11)	Lower limit on $L_{Si}\delta$ (mol^2/J per s) using $\gamma = 0{\cdot}3$ J/m^2
300 (aqueous)	Iishi *et al.* (1997)	haematite + amorphous SiO_2	~0·02	—	0·4	—	—
600–700	Khisina *et al.* (1995, 1998)	Magnesioferrite ($MgFe_2O_4$) + magnetite + (?)SiO_2	0·005–0·006	—	0·2?	—	—
650	Champness (1970, Fig. 5)	haematite + amorphous SiO_2	≈0·01	$1{\cdot}4 \times 10^{-13}$	0·3	$7{\cdot}7 \times 10^{-31}$	$2{\cdot}6 \times 10^{-30}$
770	Mackwell (1992)	Fe oxide + SiO_2	≪1	$(1–6) \times 10^{-10}$	—	—	—
800	Kondoh *et al.* (1985)	haematite + magnetite + amorphous SiO_2	0·014	—	0·5	—	—
800–950	Champness (1970)	magnetite + SiO_2	0·015	—	0·6	—	—
900	Kohlstedt & Vander Sande (1975, Fig. 6), Kohlstedt *et al.* (1976)	haematite or magnetite + SiO_2	≈0·02	$6{\cdot}9 \times 10^{-11}$	0·8	3×10^{-27}	1×10^{-26}
1030	Mackwell (1992)	Fe oxide + SiO_2	<1	$3{\cdot}6 \times 10^{-9}$	—	—	—
1050	Champness (1970, Fig. 7)	haematite + poorly crystalline SiO_2	≈0·2	—	8	—	—
1060	Brewster & O'Reilly (1988, plate 1b)	magnetite + cristobalite	≈0·3	$>10^{-10}$	13	—	—
1120	Brewster & O'Reilly (1988, plate 1c)	magnetite + cristobalite	≈1	$2{\cdot}9 \times 10^{-11}$	44	2×10^{-22}	7×10^{-22}

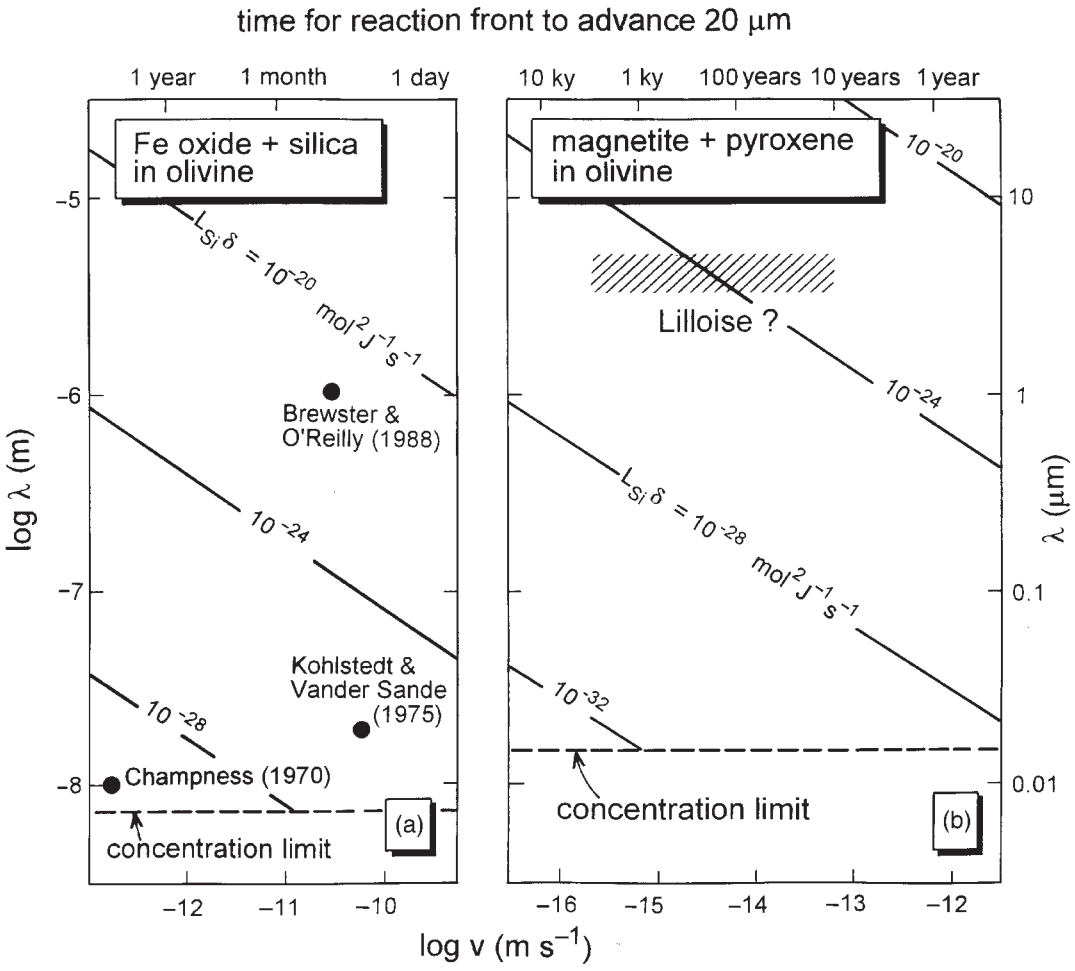

Fig. 6. Interpretation of the lamellar symplectites in olivine. Contours of $L_{Si}\delta$ are calculated from equation (11) using the value 0·3 J/m^2 for grain-boundary energy γ in the symplectite. The value of λ corresponding to the concentration limit for Si is calculated from inequality (12) with $T = 1000$°C. (a) Oxidation reaction ($p_L = 0{\cdot}5$, $K = 1{\cdot}1 \times 10^7$ mol^2/m^6), with experimental results from Table 2 plotted. (b) Exsolution reaction ($p_L = 0{\cdot}25$, $K = 2{\cdot}8 \times 10^6$ mol^2/m^6), showing the range of suggested timescale of reaction in the Lilloise intrusion, if $L_{Si}\delta$ was between $\sim 10^{-23}$ (corresponding to $T \approx 1000$°C) and $\sim 10^{-25}$ mol^2/J per s (corresponding to an upper limit of a few thousand years for the timescale).

& Ashworth, 1983). The symplectite has rod geometry (Fig. 8).

The estimate for $L_{Si}\delta/v$ comes from previous work. Using the slight zoning of hornblende across the monomineralic layer as a measure of minimum concentration gradient for Al in the grain boundaries, Ashworth (1993) estimated a maximum value for $(D_{Al})_{eff}.t$, where $(D_{Al})_{eff}$ is the effective or bulk diffusion coefficient for Al and t is the duration of reaction. Following the reasoning of Ashworth & Sheplev (1997, p. 3681), this gives a maximum estimate for $(L_{Si})_{eff}.t$, $\sim 3{\cdot}8 \times 10^{-10}$ mol^2/J per m, corresponding to a minimum overstep of equilibrium temperature (by ~ 100°C), and minimum estimate for $(-\Delta G)_{ext}$ (≈ 10 kJ per mole of symplectite produced). It is not possible that $(L_{Si})_{eff}.t$ was an order of magnitude smaller than this, because the temperature overstep would become geologically impossible (many hundreds of degrees). It is conceivable that concentration gradients were even smaller than considered above, in which case $(L_{Si})_{eff}.t$ is underestimated, and $(-\Delta G)_{ext}$ is overestimated by the same factor. However, Ashworth *et al.* (1998, p. 245), comparing the present reaction at $T \approx 600$°C with a granulite-facies one at $T \approx 720$°C, noted that the suggested difference in $(L_{Si})_{eff}$ is consistent with experimental activation energies for grain-boundary diffusion in this temperature range (Farver & Yund, 1995, 1996).

During time t, the reaction front advanced into plagioclase by a distance of typically 100 μm. Although growth rate should decrease parabolically with time (Ashworth & Sheplev, 1997), three-quarters of the symplectite should have grown at a rate within a factor of two of $(100/t)$ μm/s. Thus dividing $(L_{Si})_{eff}.t$ by 100 μm gives, as

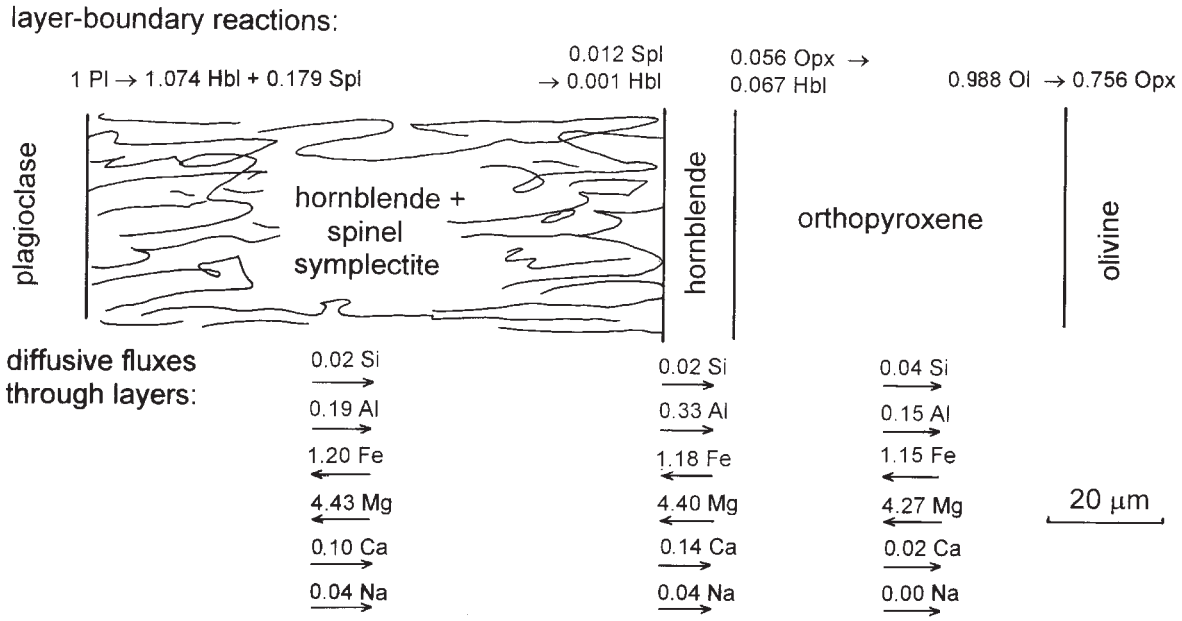

Fig. 7. Diagram of a corona modelled by Ashworth & Sheplev (1997) in rocks described by Mongkoltip & Ashworth (1983). A layer of hornblende–spinel symplectite has formed adjacent to reactant plagioclase. The reactions at each contact, and the corresponding fluxes of elements across each layer, are taken from Ashworth & Sheplev (1997, table A3). (The frame of reference for the fluxes is given by the instantaneous positions of the layer boundaries.)

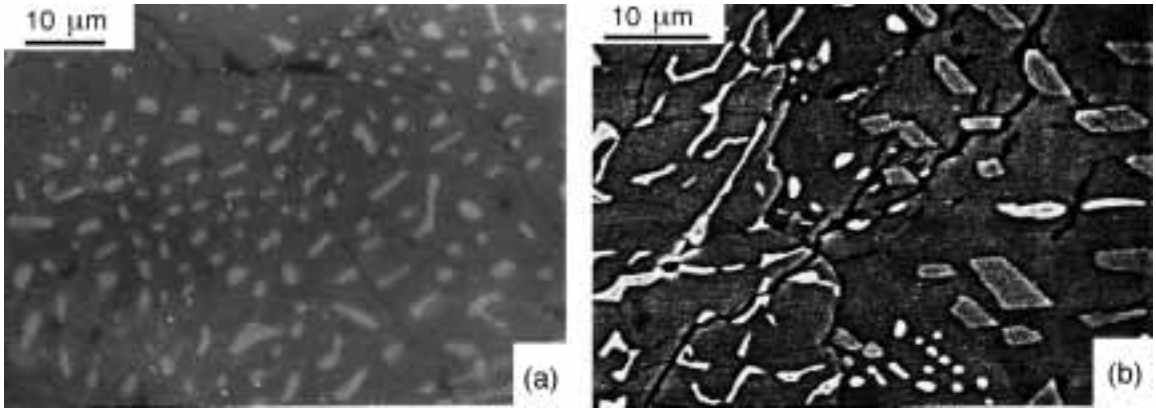

Fig. 8. Rod symplectites in troctolite from Belhelvie, NE Scotland. (a) Hornblende–spinel symplectite, forming the hornblende–spinel layer of Fig. 7, in which spinel (lighter) is the rod mineral. Many rods are sectioned approximately perpendicular to length, and show nearly circular cross-sections. (Reflected light, oil immersion.) (b) A more complex area in backscattered electron image (from Mongkoltip & Ashworth, 1983, Fig. 4f). In hornblende–spinel symplectite (left), the spinel rods (bright) are sectioned oblique to length and therefore show elongation. In anorthite–hornblende symplectite (right), polygonal hornblende is the minor or rod mineral. This area of anorthite–hornblende symplectite is unusual in also containing blebs of spinel.

a viable approximation, $(L_{Si})_{eff}/v \approx 3{\cdot}8 \times 10^{-6}$ mol^2/J per m. The approximate relation between $(L_{Si})_{eff}$ and $L_{Si}\delta$ is

$$(L_{Si})_{eff} = 2\,N L_{Si}\delta$$

where N is the number of grain boundaries per metre of line transect (Ashworth *et al.*, 1998). Measurements give $N \approx 3 \times 10^4$ m^{-1} in the hornblende layer (Ashworth, 1993), leading to $L_{Si}\delta/v \approx 6{\cdot}3 \times 10^{-11}$ mol^2/J per m.

The value of K is to be estimated next. Following the previous diffusion modelling by Ashworth & Birdi (1990) and Ashworth & Sheplev (1997), 24-oxygen moles are used for all minerals. For each mole of plagioclase consumed, more than one mole of symplectite is produced (Fig. 7), because material diffuses along grain boundaries

Table 3: Calculation of K for hornblende-spinel and anorthite–hornblende symplectites

	Mineral compositions (moles element per 24-oxygen mole of mineral)							
	Si	Al	Fe	Mg	Ca	Na	p_j	ν_j
Plagioclase (reactant):	6·68	5·32	—	—	2·32	0·68	—	1·000
Spl:	—	12·00	2·40	3·60	—	—	0·127	−0·179
Hbl1 (with Spl):	6·20	2·78	0·72	3·53	1·85	0·66	0·873	−1·074
Hbl2 (with An):	6·61	2·20	0·66	3·73	1·84	0·44	0·250	−0·265
An:	6·15	5·85	—	—	2·85	0·15	0·750	−0·794
For Hbl1 + Spl symplectite (V = 2·71 × 10^{-4} m^3/mol)								
k values (× 10^{-4}) mol/m^3								
$(k_{Spl})_i$	1·97	−3·36	−0·99	−1·48	0·68	0·20		
$(k_{Hbl1})_i$	−0·28	0·56	−0·26	−1·28	0·01	−0·04		
Using L_{Si}/L_{Al} = 0·1, L_{Si}/L_i = 0·012 (i = Fe, Mg, Ca, Na):								
$p_{Spl}^2 (k_{Spl})_i^2 (L_{Si}/L_i)$ (× 10^{-5}) mol^2/m^6	62·42	18·19	0·19	0·42	0·09	0·01		
$(4p_{Spl} - p_{Spl}^2 - 2 \ln p_{Spl} - 3) (k_{Hbl1})_i^2 (L_{Si}/L_i)$ (× 10^{-5}) mol^2/m^6	126·03	50·68	1·32	31·78	0·00	0·03		
K = 9·10 × 10^5 mol^2/m^6, from equation (A2)								
For An + Hbl2 symplectite (V = 2·96 × 10^{-4} m^3/mol)								
k values (× 10^{-4}) mol/m^3								
$(k_{Hbl2})_i$	−0·10	0·95	−0·22	−1·26	0·12	0·07		
$(k_{An})_i$	0·05	−0·27	0·00	0·00	−0·22	0·17		
Using L_{Si}/L_{Al} = 0·1, L_{Si}/L_i = 0·012 (i = Fe, Mg, Ca, Na):								
$p_{Hbl2}^2 (k_{Hbl2})_i^2 (L_{Si}/L_i)$ (× 10^{-5}) mol^2/m^6	0·68	5·68	0·04	1·19	0·01	0·00		
$(4p_{Hbl2} - p_{Hbl2}^2 - 2 \ln p_{Hbl2} - 3) (k_{An})_i^2 (L_{Si}/L_i)$ (× 10^{-5}) mol^2/m^6	2·02	5·53	0·00	0·00	0·42	0·25		
K = 4·94 × 10^4 mol^2/m^6, from equation (A2)								

Spl, spinel; Hbl, hornblende; An, anorthite. Mineral compositions from Mongkoltip & Ashworth (1983) and Ashworth & Sheplev (1997). Volume proportions p_j from Mongkoltip & Ashworth (1983). Reaction coefficients ν_j from Ashworth & Sheplev (1997) for Hbl1 + Spl, and by assumption of approximate Al, Si retention in An + Hbl2.

through the corona to the symplectite-forming reaction front. (Implicit in this is that oxygen diffuses along with the cations. Oxygen diffusion is not treated explicitly in the modelling, where the components are oxides, so that Si stands for SiO_2. Relatively easy oxygen diffusion, in comparison with the reaction in olivine, is consistent with the generally non-coherent nature of grain boundaries in the coronas.) This addition of material is incorporated into the calculation of K, by using the stoichiometric coefficients ν_j of the minerals and their molar contents n_{ij} of components i. Diffusion to the reaction front being predominantly grain-boundary diffusion through the symplectite layer, diffusion through bulk minerals is neglected: addition or subtraction of component i at the reaction front is due solely to the local reaction. Advance of the reaction front by 1 m corresponds to production of $1/V$ moles of symplectite per m^2 and consumption of $(-\nu_{Pl}/\Sigma\nu_j)/V$ moles of plagioclase, where ν_{Pl} is the stoichiometric coefficient of plagioclase and the summation is over the product minerals. This releases $(-\nu_{Pl}/\Sigma\nu_j)\, ni_{Pl}/V$ moles of component i. The proportion of the reaction front at which mineral j is growing is p_j. The deposition of component i in mineral j corresponding to the above release from plagioclase is $(\nu_j/p_j\Sigma\nu_j)n_{ij}/V$. Thus

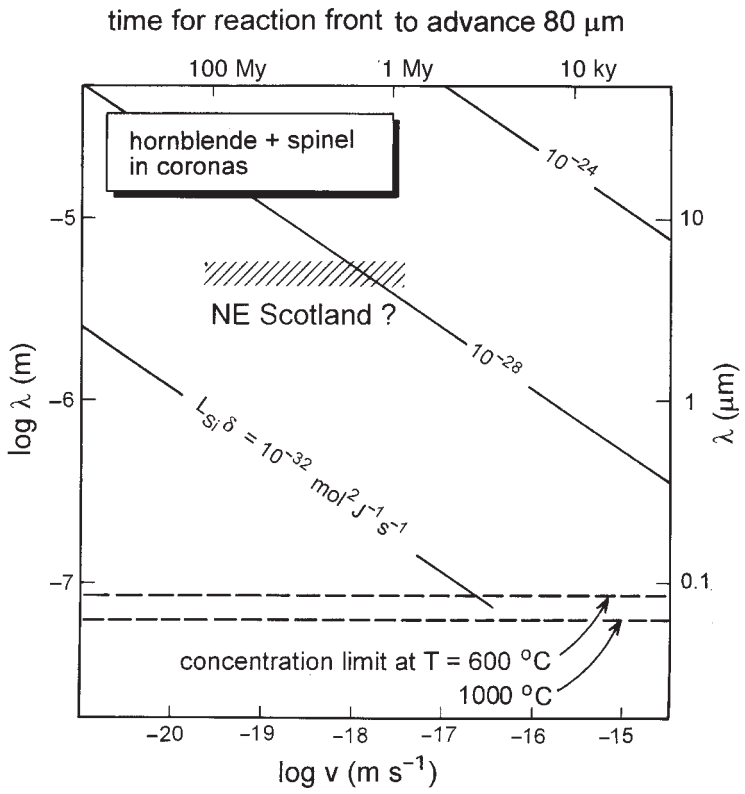

Fig. 9. Interpretation of the hornblende + spinel rod symplectite of Figs 7 and 8, with $p_R = 0{\cdot}127$, $K = 9{\cdot}1 \times 10^5$ mol^2/m^6. Contours of $L_{Si}\delta$ are calculated from equation (11) with $\gamma = 1{\cdot}3$ J/m^2. The timescale of reaction is assumed to be in the range ~ 1 to ~ 100 My. The value of λ corresponding to the concentration limit for Si is calculated from inequality (13). The concentration limit calculated for Al is slightly less constraining ($1{\cdot}7 \times 10^{-8}$ and $1{\cdot}1 \times 10^{-8}$ m at 600 and 1000°C, respectively).

the net addition of component i to the reaction front where j is growing is given by

$$(k_j)_i = -\frac{1}{V\Sigma\,\nu_j}\left((\nu_{Pl}\,n_{i\,Pl} + \frac{\nu_j}{p_j}\,n_{ij}\right).$$

Table 3 shows $(k_j)_i$ values, leading to K from equation (A2) of the Appendix.

The above working follows corona models using $L_{Si}/L_{Al} = 0{\cdot}1$ (Table 3). It is possible to model the coronas with other L_{Si}/L_{Al} ratios, as high as 0·3 and with no lower limit; L_{Si}/L_i (i = Mg, Fe, Ca, Na) then varies proportionally to L_{Si}/L_{Al} (Ashworth & Sheplev, 1997, Fig. 3). So, approximately, does the value estimated for $L_{Si}\delta/v$; thus the ratio of the two that appears in $L_{Si}\delta/Kv$ for equation (11) varies relatively little, and trial calculations indicate that the estimates presented here are reliable to within a factor of two, provided that $L_{Si}/L_{Al} > 0{\cdot}03$. It seems unlikely that the two diffusion coefficients differ by more than an order of magnitude, given that both Si and Al diffuse within the reaction front but hardly at all beyond it (Mongkoltip & Ashworth, 1983).

The remaining quantity required is λ, which is measured in micrographs such as Fig. 8. If n rods are counted in an area A m^2, each rod being associated with an area of approximately $\pi(\lambda/2)^2$, the estimate for λ is

$$\lambda = 2\left(\frac{A}{\pi\,n}\right)^{1/2}.$$

The average result is $5{\cdot}0 \pm 0{\cdot}5$ μm from 322 rods. Micrographs giving anomalously large λ (up to 11 μm) were discounted as probably from sections cut misleadingly oblique to the rods, or material coarsened after growth. This is supported by the following observation on the anorthite–hornblende symplectite, which occurs as patches adjacent to the hornblende–spinel (Fig. 8b). The geometry is more regular, and consistently gives $\lambda = 10{\cdot}0 \pm 0{\cdot}4$ μm. It has a smaller K because Al and Si are less strongly separated than in hornblende–spinel (Table 3). The factor of ~ 18 in K suggests a factor of $(18)^{1/3} = 2{\cdot}6$ in λ if v was the same, which compares well with the factor of 2·0 in the above data.

Using all the above information, the result for γ from equation (11) is 1·3 J/m^2. This is an order-of-magnitude

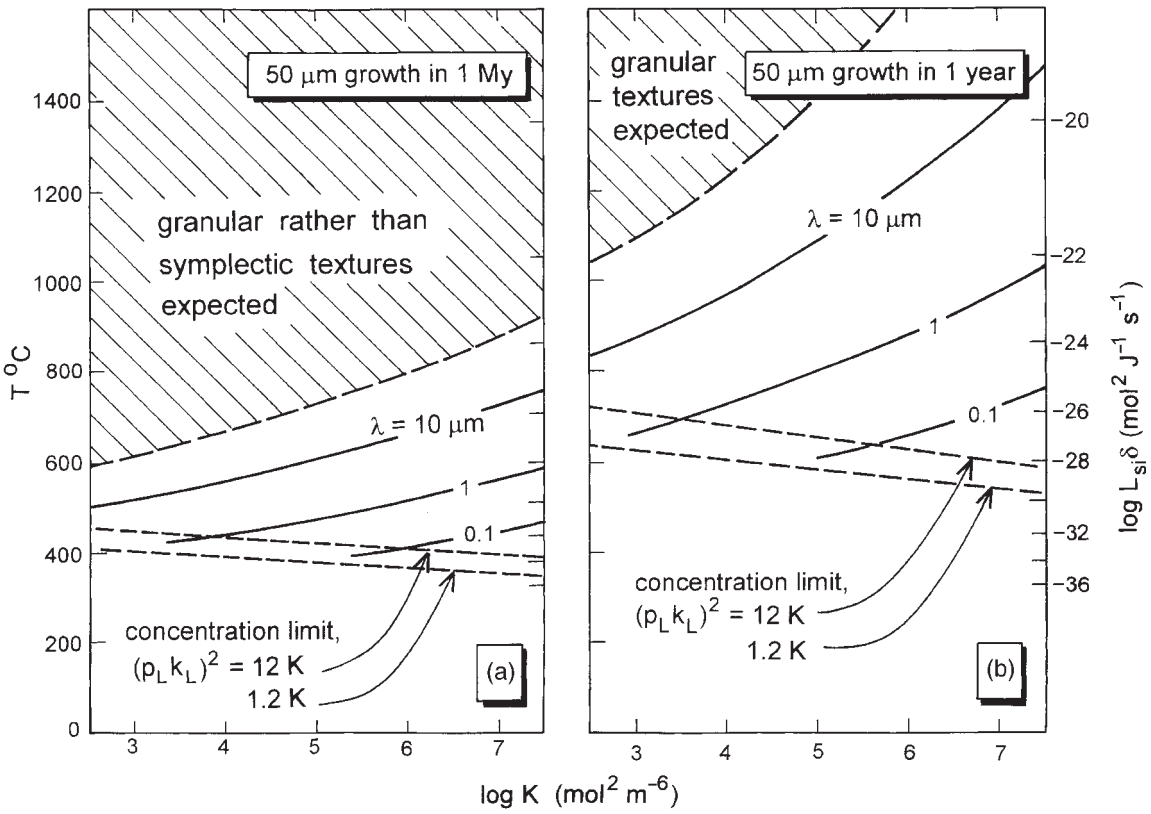

Fig. 10. Synoptic diagrams for generalized production of lamellar symplectites (or, equivalently, rod symplectites with $p_R = 0{\cdot}25$), in a case of (a) slow reaction, duration 1 My, representative of regional metamorphism, and (b) fast reaction, duration 1 year, as might occur in fast-cooling igneous rocks. Grain-boundary energy γ is set at 0·5 J/m^2, and $L_{Si}\delta$ is taken to be 10^{-28} m^3/s at 600°C with activation energy 300 kJ/mol. Granular textures are expected where the intergrowth spacing λ becomes larger than the growth dimension of the symplectite, which is set at 50 μm. Concentration limits, for Si as limiting element, are calculated from inequality (12). That for a lamellar symplectite with $(p_L k_L)^2 = 12K$ refers to Si-dominated energy dissipation in the reaction front and no external diffusion of Si, and is also valid for a rod symplectite with $p_R = 0{\cdot}25$ under the same conditions. The concentration limit with smaller ratio of $(p_L k_L)^2$ to K could be appropriate for a more complex reaction.

estimate only, but is satisfactorily within the range of values indicated by the literature reviewed in the last section. The measurement of λ is one obvious possible source of error. Errors could also arise in $L_{Si}\delta/v$; if the estimate of $(-\Delta G)_{ext}$ is too large, or if $L_{Si}\delta$ in the reaction front is larger than in grain boundaries within layers, then the value used for $L_{Si}\delta/v$ will be too small and the estimate of γ too large. Using $\gamma = 1{\cdot}3$ J/m^2, Fig. 9 shows the suggested ranges of $L_{Si}\delta$ for the reaction, and also that the concentration limit was not approached.

The amount of free energy driving reaction-front processes can be estimated:

$$(-\Delta G)_{rf} = 2\,(-\Delta G)_{gb} = \frac{8\sqrt{(p_R)}\gamma V}{\lambda}. \qquad (18)$$

This gives $(-\Delta G)_{rf} \approx 200$ J/mol, or roughly 2% of the estimate of 10 kJ/mol for $(-\Delta G)_{ext}$. Only a very small proportion of the overall affinity of the corona-forming reaction was associated with the symplectite-forming reaction front. This is a firm conclusion, being insensitive to errors in $(-\Delta G)_{ext}$ because the estimate for γ is inversely proportional to that for $L_{Si}\delta/v$ [equation (11)] and hence proportional to that for $(-\Delta G)_{ext}$. This result justifies neglecting $(-\Delta G)_{rf}$ in the diffusion modelling of the overall reaction (Ashworth & Sheplev, 1997).

CONCLUSIONS

The theory developed here seems adequate to explain the spacings in symplectites if grain-boundary energies of minerals are $\sim 0{\cdot}1$ to ~ 1 J/m^2, in agreement with estimates by other techniques. Symplectites with similar spacings, λ, can grow in a wide range of different environments. It is striking that the two examples studied here, one from a shallow intrusion and the other from a regional metamorphic setting, have nearly identical spacings despite what must have been very different reaction rates. This is explained mainly by a much smaller diffusion coefficient $L_{Si}\delta$ accompanying the slower rate

v, as a result of the lower temperature. On the other hand, spacings can be similar over large ranges of temperature and reaction rate, because λ depends on the cube root of $L_{Si}\delta/v$. (The use of Si as reference element is appropriate because of its major influence on the common symplectites studied here, but other elements would be more appropriate in some cases.) For given K, v and δ, symplectites having λ within an order of magnitude of 1 μm can grow over a range of six orders of magnitude for the diffusion coefficient L_{Si}. This is illustrated in Fig. 10, for what may (in the light of this study) be a typical value of γ (0·5 J/m^2) and a typical range of $L_{Si}\delta$. The latter is set at 10^{-28} mol^2/J per s at 600°C (see Fig. 9), with temperature dependence governed by an activation energy of 300 kJ/mol, this being about mid-range among estimates from grain-boundary diffusion experiments (Yund, 1997, Fig. 4). A reaction front with these or similar diffusion properties may contain dissolved H_2O (Yund, 1997), but is certainly solid. In the presence of a fluid phase, symplectic reaction is much less likely. This is not only because diffusion coefficients are much greater, but also because diffusion geometry should be much less regular, through a fluid distributed unevenly in pores, pockets or microcracks. It is unlikely that a fluid would occupy an entire reaction front uniformly, allowing diffusion strictly perpendicular to the grain-boundaries of a growing symplectite.

In addition to temperature, and probably H_2O content of the reaction front, another factor influencing whether a symplectite forms is K of the potential reaction (Fig. 10). It ranges from 5×10^4 to 1×10^7 mol^2/m^6 in this study (Fig. 6, Table 3). If the product minerals are very different in composition, particularly for slow-diffusing elements, then K is large, and this will favour symplectic rather than granular texture (Fig. 10). This is a more general criterion for symplectite formation than that of Mongkoltip & Ashworth (1983), that two slow-diffusing species are usually involved.

Selected concentration limits are shown in Fig. 10. The upper line represents the limiting case with only Si contributing to K, in a system closed to Si [equation (15)]. A reaction in which other elements also contribute to K could have a larger ratio of K to $(p_L k_L)^2$ for Si, as exemplified by the limit shown for one order of magnitude larger ratio. The concentration limit should tend to inhibit symplectite production at low T, as also will the requirement for large $(-\Delta G)$: the free energy required in the reaction front, $(-\Delta G)_{rf}$, is inversely proportional to λ, as can be seen from equation (18) or its lamellar equivalent with 4 in place of $8\sqrt{(p_R)}$. At temperatures too low for symplectite formation, there may be no reaction at all (in the absence of fluid). Alternatively, if $(-\Delta G)$ is sufficient, there may be a highly metastable reaction avoiding the diffusion required for the symplectite: in the oxidation of olivine, laihunitization may play this role. At higher temperatures, in a broad swathe of igneous and metamorphic settings, symplectites are the predictable products of many diffusive, solid-state reactions.

ACKNOWLEDGEMENTS

Dr V. S. Sheplev introduced J.R.A. to the principle of maximum rate of energy dissipation. The paper benefited from critical review by C. T. Foster and an anonymous referee. TEM work was done in the School of Metallurgy and Materials, University of Birmingham, by courtesy of Professor M. H. Loretto.

REFERENCES

Abdou, S., Solórzano, G., El-Boragy, M., Gust, W. & Predel, B. (1996). *In-situ* study of discontinuous precipitation in Al-15 at. % Zn. *Scripta Materialia* **34**, 1431–1436.

Ashworth, J. R. (1993). Fluid-absent diffusion kinetics of Al inferred from retrograde metamorphic coronas. *American Mineralogist* **78**, 331–337.

Ashworth, J. R. & Birdi, J. J. (1990). Diffusion modelling of coronas around olivine in an open system. *Geochimica et Cosmochimica Acta* **54**, 2389–2401.

Ashworth, J. R. & Sheplev, V. S. (1997). Diffusion modelling of metamorphic layered coronas with stability criterion and consideration of affinity. *Geochimica et Cosmochimica Acta* **61**, 3671–3689.

Ashworth, J. R., Birdi, J. J. & Emmett, T. F. (1992). Diffusion in coronas around clinopyroxene: modelling with local equilibrium and steady state, and a non-steady-state modification to account for zoned actinolite–hornblende. *Contributions to Mineralogy and Petrology* **109**, 307–325.

Ashworth, J. R., Sheplev, V. S., Bryxina, N. A., Kolobov, V. Yu. & Reverdatto, V. V. (1998). Diffusion-controlled corona reaction and overstepping of equilibrium in a garnet granulite, Yenisey Ridge, Siberia. *Journal of Metamorphic Geology* **16**, 231–246.

Bögel, A. & Gust, W. (1988). A standardized model and a reaction principle for discontinuous precipitation. *Zeitschrift für Metallkunde* **79**, 296–306.

Boland, J. N. & Otten, M. T. (1985). Symplectitic augite: evidence for discontinuous precipitation as an exsolution mechanism in Ca-rich clinopyroxene. *Journal of Metamorphic Geology* **3**, 13–20.

Boland, J. N. & van Roermund, H. L. M. (1983). Mechanisms of exsolution in omphacites from high temperature, type B, eclogites. *Physics and Chemistry of Minerals* **9**, 30–37.

Brewster, D. & O'Reilly, W. (1988). Magnetic properties of synthetic analogues of the altered olivines of igneous rocks. *Geophysical Journal* **95**, 421–432.

Cahn, J. W. (1959). The kinetics of cellular segregation reactions. *Acta Metallurgica* **7**, 18–28.

Cameron, M. & Papike, J. J. (1981). Structural and chemical variations in pyroxenes. *American Mineralogist* **66**, 1–50.

Chambers, A. D. & Brown, P. E. (1995). The Lilloise intrusion, East Greenland: fractionation of a hydrous alkali picritic magma. *Journal of Petrology* **36**, 933–963.

Champness, P. E. (1970). Nucleation and growth of iron oxides in olivines, $(Mg,Fe)_2SiO_4$. *Mineralogical Magazine* **37**, 790–800.

Cooper, R. F. & Kohlstedt, D. L. (1982). Interfacial energies in the olivine-basalt system. In: Akimoto, S. & Manghnani, M. H. (eds)

High-Pressure Research in Geophysics. Tokyo: Center for Academic Publications, pp. 217–228.

Deer, W. A., Howie, R. A. & Zussman, J. (1982). *Rock-forming Minerals. Vol. 1A. Orthosilicates*, 2nd edn. Harlow, UK: Longman.

Duly, D., Cheynet, M. C. & Brechet, Y. (1994). Morphology and chemical nanoanalysis of discontinuous precipitation in Mg–Al alloys—I. Regular growth. *Acta Metallurgica et Materialia* **42**, 3843–3854.

Farver, J. R. & Yund, R. A. (1995). Grain boundary diffusion of oxygen, potassium and calcium in natural and hot-pressed feldspar aggregates. *Contributions to Mineralogy and Petrology* **118**, 340–355.

Farver, J. R. & Yund, R. A. (1996). Volume and grain boundary diffusion of calcium in natural and hot-pressed calcite aggregates. *Contributions to Mineralogy and Petrology* **123**, 77–91.

Farver, J. R., Yund, R. A. & Rubie, D. C. (1994). Magnesium grain boundary diffusion in forsterite aggregates at 1000°–1300°C and 0·1 MPa to 10 GPa. *Journal of Geophysical Research B* **99**, 19809–19819.

Fisher, G. W. & Lasaga, A. C. (1981). Irreversible thermodynamics in petrology. *Reviews in Mineralogy* **8**, 171–209.

Fisler, D. K. & Mackwell, S. J. (1994). Kinetics of diffusion-controlled growth of fayalite. *Physics and Chemistry of Minerals* **21**, 156–165.

Fisler, D. K., Mackwell, S. J. & Petsch, S. (1997). Grain boundary diffusion in enstatite. *Physics and Chemistry of Minerals* **24**, 264–273.

Haggerty, S. E. & Baker, I. (1967). The alteration of olivine in basaltic and associated lavas. Part I: High temperature alteration. *Contributions to Mineralogy and Petrology* **16**, 233–257.

Hay, R. S. & Evans, B. (1988). Intergranular distribution of pore fluid and the nature of high-angle grain boundaries in limestone and marble. *Journal of Geophysical Research B* **93**, 8959–8974.

Holland, T. J. B. & Powell, R. (1998). An internally consistent thermodynamic data set for phases of petrological interest. *Journal of Metamorphic Geology* **16**, 309–343.

Houlier, B., Cheraghmakani, M. & Jaoul, O. (1990). Silicon diffusion in San Carlos olivine. *Physics of the Earth and Planetary Interiors* **62**, 329–340.

Iishi, K., Torigoe, K. & Han, X. J. (1997). Oriented precipitate complexes in iron-rich olivines produced experimentally in aqueous oxidizing environment. *Physics and Chemistry of Minerals* **25**, 8–14.

Johnston, A. D. & Stout, J. H. (1984). Development of orthopyroxene–Fe/Mg ferrite symplectites by continuous olivine oxidation. *Contributions to Mineralogy and Petrology* **88**, 196–202.

Khisina, N. R., Khramov, D. A., Kolosov, M. V., Kleschev, A. A. & Taylor, L. A. (1995). Formation of ferriolivine and magnesioferrite from Mg–Fe-olivine: reactions and kinetics of oxidation. *Physics and Chemistry of Minerals* **22**, 241–250.

Khisina, N. R., Khramov, D. A., Kleschev, A. A. & Langer, K. (1998). Laihunitization as a mechanism of olivine oxidation. *European Journal of Mineralogy* **10**, 229–238.

Kohlstedt, D. L. & Vander Sande, J. B. (1975). An electron microscopy study of naturally occurring oxidation produced precipitates in iron-bearing olivines. *Contributions to Mineralogy and Petrology* **53**, 13–24.

Kohlstedt, D. L., Goetze, C., Durham, W. B. & Vander Sande, J. (1976). New technique for decorating dislocations in olivine. *Science* **191**, 1045–1046.

Kondoh, S., Kitamura, M. & Morimoto, N. (1985). Synthetic laihunite ($\square_x Fe^{2+}_{2-3x}Fe^{3+}_{2x}SiO_4$), an oxidation product of olivine. *American Mineralogist* **70**, 737–746.

Kretz, R. (1994). *Metamorphic Crystallization*. Chichester, UK: John Wiley.

Mackwell, S. J. (1992). Oxidation kinetics of fayalite (Fe_2SiO_4). *Physics and Chemistry of Minerals* **19**, 220–228.

Mongkoltip, P. & Ashworth, J. R. (1983). Quantitative estimation of an open-system symplectite-forming reaction: restricted diffusion of Al and Si in coronas around olivine. *Journal of Petrology* **24**, 635–661.

Morioka, M. & Nagasawa, H. (1991). Ionic diffusion in olivine. In: Ganguly, J. (ed.) *Diffusion, Atomic Ordering and Mass Transport: Selected Topics in Geochemistry*. Berlin: Springer-Verlag, pp. 176–197.

Moseley, D. (1984). Symplectic exsolution in olivine. *American Mineralogist* **69**, 139–153.

Nakamura, A. & Schmalzried, H. (1983). On the nonstoichiometry and point defects of olivine. *Physics and Chemistry of Minerals* **10**, 27–37.

Otten, M. T. (1985). The subsolidus history of the Artfjället gabbro: a TEM study of olivine, augite and orthopyroxene. *Journal of Petrology* **26**, 488–514.

Penn, R. L., Banfield, J. F. & Kerrick, D. M. (1999). TEM investigation of Lewiston, Idaho, fibrolite: microstructure and grain boundary energetics. *American Mineralogist* **84**, 152–159.

Putnis, A. (1979). Electron petrography of high-temperature oxidation in olivine from the Rhum Layered Intrusion. *Mineralogical Magazine* **43**, 293–296.

Rietmeijer, F. J. M. (1996). Cellular precipitates of iron oxide in olivine in a stratospheric interplanetary dust particle. *Mineralogical Magazine* **60**, 877–885.

Sederholm, J. J. (1916). On synantetic minerals and related phenomena (reaction rims, corona minerals, kelyphite, myrmekite &c.). *Bulletin de la Commission Géologique de Finlande* **48**.

Solorzano, I. G. & Purdy, G. R. (1984). Interlamellar spacing in discontinuous precipitation. *Metallurgical Transactions A* **15**, 1055–1063.

Spry, A. (1969). *Metamorphic Textures*. Oxford: Pergamon Press.

Voll, G. (1982). Wechselsäume und zelluläre Verwachsungen: Bildung, Morphologie und kinetische Aspekte. *Fortschritte der Mineralogie* **60**, 207–210.

Yund, R. A. (1997). Rates of grain boundary diffusion through enstatite and forsterite reaction rims. *Contributions to Mineralogy and Petrology* **126**, 224–236.

Zieba, P. & Gust, W. (1998). Analytical electron microscopy of discontinuous solid state reactions. *International Materials Reviews* **43**, 70–97.

APPENDIX: ENERGY TERMS FOR ROD GEOMETRY

An idealized geometry of a rod symplectite comprises hexagonal domains (Fig. A1a), although in reality they are less regular (Fig. 8). As an approximation, a circular geometry is used (Fig. A1b). The area $\pi(\lambda/2)^2$ contains length $\pi\lambda\sqrt{p_R}$ of grain boundary, where p_R is the volume proportion of the rod mineral. The grain boundary energy per mole is thus

$$(-\Delta G)_{gb} = \frac{4\sqrt{(p_R)}\gamma V}{\lambda}.$$

We let the effective difference in concentration of an element between reactant mineral and rod product be k_R (analogous to k_L for lamellae), and k_H is still the analogous difference between reactant and host product. Flux at distance r from the centre of a rod is

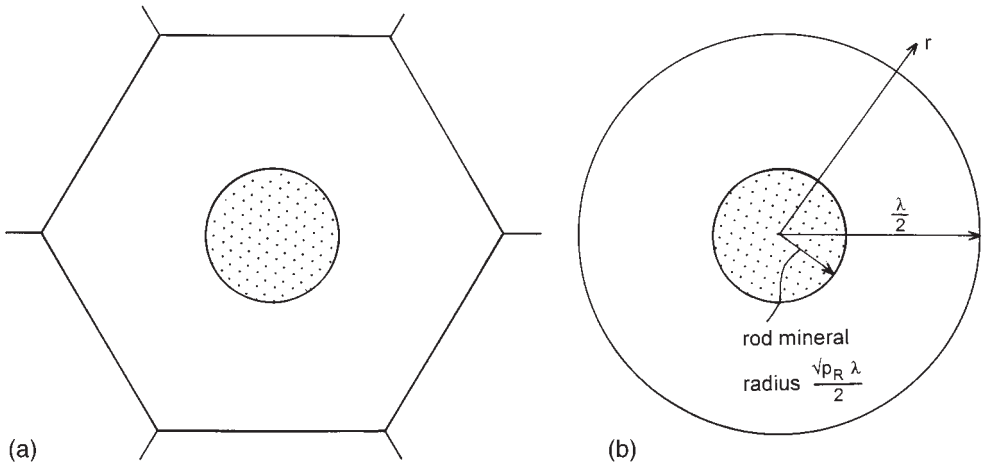

Fig. A1. Geometry of rod symplectite. (a) Idealized hexagonal region of host mineral surrounding a rod. (b) Simplified geometry used in this paper.

$$\mathcal{J} = \frac{vk_{\mathrm{R}}r}{2\delta} \qquad [0 \le r \le \sqrt{(p_{\mathrm{R}}}\lambda/2)]$$

$$\mathcal{J} = \frac{-vk_{\mathrm{H}}}{2\delta}\left(\frac{\lambda^2}{4r} - r\right) \qquad [\sqrt{(p_{\mathrm{R}})}\lambda/2 \le r \le \lambda/2].$$

Assuming Fick's Law, concentration varies thus:

$$c = c_0 - \frac{v\,k_{\mathrm{R}}r^2}{4D\delta} \qquad [0 \le r \le \sqrt{(p_{\mathrm{R}})}\lambda/2]$$

$$c = c_0 - \frac{v\,k_{\mathrm{R}}p_{\mathrm{R}}\lambda^2}{16\,D\,\delta} + \frac{v\,k_{\mathrm{H}}}{2\,D\,\delta}\left\{\frac{\lambda^2}{8}\left[p_{\mathrm{R}} - 2\ln\frac{\sqrt{(p_{\mathrm{R}})}\lambda}{2\,r}\right] - \frac{r^2}{2}\right\}$$
$$[\sqrt{(p_{\mathrm{R}})}\lambda/2 \le r \le \lambda/2].$$

The minimum concentration (at $r = \lambda/2$) for an element diffusing from rod to host is

$$c_{\min} = c_0 - \frac{v\,\lambda^2}{16\,D\,\delta}[k_{\mathrm{R}}\,p_{\mathrm{R}} - k_{\mathrm{H}}\,(p_{\mathrm{R}} - \ln p_{\mathrm{R}} - 1)]$$

and the equivalent of concentration limit (4) is

$$\frac{L\delta}{v} > \frac{\lambda^2}{16\,RT}[k_{\mathrm{R}}\,p_{\mathrm{R}} - k_{\mathrm{H}}\,(p_{\mathrm{R}} - \ln p_{\mathrm{R}} - 1)]. \quad \text{(A1)}$$

The rate of energy dissipation per unit volume of reaction front is

$$\mathcal{T}\sigma = \frac{v^2k_{\mathrm{R}}{}^2r^2}{4\,L\,\delta^2} \qquad [0 \le r \le \sqrt{(p_{\mathrm{R}})}\lambda/2]$$

$$\mathcal{T}\sigma = \frac{v^2k_{\mathrm{H}}{}^2}{4\,L\,\delta^2}\left(\frac{\lambda^2}{4r} - r\right)^2 \qquad [\sqrt{(p_{\mathrm{R}})}\lambda/2 \le r \le \lambda/2].$$

Multiplying by $\delta.2\pi r.\mathrm{d}r$ and integrating from $r = 0$ to $r = \lambda/2$ gives the energy dissipation rate in an area $\pi(\lambda/2)^2$ of reaction front. Then dividing by $v\pi(\lambda/2)^2/V$ gives

$$(-\Delta G)_{\mathrm{diff}} = \frac{2\,v\,V}{\lambda^2 L\delta}\left[k_{\mathrm{R}}{}^2\int_0^{\sqrt{(p_{\mathrm{R}})}\lambda/2} r^3\mathrm{d}r + k_{\mathrm{H}}{}^2\int_{(p_{\mathrm{R}})}^{\lambda/2}\left(\frac{\lambda^2}{4r} - r\right)^2 r\,\mathrm{d}r\right]$$

$$= \frac{v\,V\lambda^2}{32\,L\,\delta}[p_{\mathrm{R}}{}^2k_{\mathrm{R}}{}^2 + (4p_{\mathrm{R}} - p_{\mathrm{R}}{}^2 - 2\ln p_{\mathrm{R}} - 3)\,k_{\mathrm{H}}{}^2]$$

for a single diffusing component. Summing over various components gives equation (5) as in the lamellar case, but with a different formula for K:

$$K = \frac{1}{32}\left[p_{\mathrm{R}}{}^2\sum_i (k_{\mathrm{R}})_i^2\frac{L_{\mathrm{Si}}}{L_i} + (4p_{\mathrm{R}} - p_{\mathrm{R}}{}^2 - 2\ln p_{\mathrm{R}} - 3)\sum_i (k_{\mathrm{H}})_i^2\frac{L_{\mathrm{Si}}}{L_i}\right] \quad \text{(A2)}$$